A study on the role of oxidative stress and protein kinase signalling in hyperglycaemia induced cardiac remodelling

By: Nikhil Amtha (AMTNIK001)

Supervisor: Associate Professor Asfree Gwanyanya

Submitted for the degree of Master of Science in Medicine specialising in Physiology (MM095 - HUB5004W)

Department of Human Biology

Faculty of Health Sciences

University of Cape Town

2023

DECLARATION

I, Nikhil Amtha, hereby declare that the work on which this dissertation/thesis is based is my original work (except where acknowledgements indicate otherwise) and that neither the whole work nor any part of it has been, is being, or is to be submitted for another degree in this or any other university.

I empower the university to reproduce for the purpose of research either the whole or any portion of the contents in any manner whatsoever.

Signature: Signed by candidate

Date: 06 August 2023

Acknowledgements

I would like to thank everyone who helped make this Master's project possible.

I would like to thank my supervisor and co-supervisor, Associate Professor Asfree Gwanyanya, and Dr. Robea Ballo, for guiding and aiding me throughout my project. I would also like to offer my gratitude to Desiree Bowers and Thulisa Mkatazo for tissue culture technical assistance. I would also like to thank my lab members in the Gwanyanya lab.

I would like to thank the National Research Foundation of South Africa (NRF freestanding scholarship) for funding my studies. I would also like to thank the funders of this study, the South African Medical Research Council (MRC Grant Number 29841).

Contents

Abstract

Background

Almost one-third of all deaths in patients with uncontrolled diabetes mellitus and hyperglycaemia are due to cardiovascular diseases. Chronic exposure of the heart to hyperglycaemia leads to a maladaptation called pathological cardiac remodelling and occurs via oxidative stress due to excess production of reactive oxygen species (ROS). In the heart, ROS modulates cardiac differentiation, cardiomyocyte proliferation, and myocardial tissue growth via ROS-sensitive protein kinases such as the mitogen-activated protein kinase (MAPK). Although there are several different MAPKs, the p38 MAPKs are involved in cardiogenesis and implicated in stimulating myocyte apoptosis, hypertrophy, or even antiapoptotic effects. As such, the role of p38 MAPKs in diabetic cardiac remodelling, especially during cardiac development, remains unclear. This study aims to elucidate the effect of hyperglycaemia on the p38 MAPK signalling pathway in a cardiac developmental model.

Methods

Pluripotent mouse embryonic stem cells (mESCs) were differentiated *in vitro* into cardiac-like pulsatile embryoid bodies (EBs) using the hanging drop method. Once pulsatile, EBs were further cultured for 72 hours in either baseline (25mM) or high glucose (50mM) media or with the pro-oxidant hydrogen peroxide (100μM). Changes in EB morphology and beating characteristics were observed using transmitted light microscopy. Immunocytochemistry and fluorescence microscopy imaging was used to detect changes in biomarkers. The nuclear uptake of propidium iodide (PI) was used to evaluate cell viability, whereas the 5-ethynyl-1-deoxyuridine (EdU) assay was used to determine cell proliferation. Western blot was used to analyse protein expression.

Results

Treatment with hydrogen peroxide stunted EB growth and decreased EB diameter, consistent with the presence of oxidative stress. High glucose increased the number of pyknotic-like nuclei and reduced the number of EdU-positive nuclei. Furthermore, hyperglycaemia elevated the expression of phosphorylated p38 MAPK, without altering total p38 MAPK expression levels. Inhibition of p38 MAPK by SB203580 in high glucose attenuated the increased number of pyknotic-like nuclei in high glucose and enhanced the number of EdU-positive nuclei compared to high glucose alone. High glucose also reduced the expression of the mitochondrial fusion regulatory protein, optic atrophy-1 (OPA1), with the inhibition of p38MAPK in high glucose attenuating this effect.

Conclusion

Hyperglycaemia induced pyknotic-like phenomenon, suppressed the proliferation, and reduced mitochondrial fusion protein machinery of mESC-derived cardiac-like cells. These effects were likely triggered by a mild form of oxidative stress and involved the activation of p38 MAPK. The findings provide insights into the mechanisms underlying diabetic developmental cardiac remodelling and identify p38MAPKs as a potential therapeutic target.

1. Introduction

1.1 Diabetes mellitus and burden of disease

Diabetes mellitus with poorly-controlled hyperglycaemia is a highly prevalent chronic metabolic disease affecting approximately 422 million people globally, with current projections expecting this number to increase to 700 million by 2045 (1). In the African context, as of 2019, according to the International Diabetes Federation, 12.8% of adults in South Africa have diabetes (2). Concerningly, 16% of live births have some form of hyperglycaemia during pregnancy, of which 84% were due to gestational diabetes (2).

Different types of diabetes mellitus include Type 1, Type 2, and gestational, depending on the pathophysiology and clinical manifestations. Type 1 diabetes, typically present in adolescence, is a T-cell autoimmune disease and is the loss of insulin-producing beta cells in the pancreas, accompanied by increased blood glucose levels (3). Type 2 is the most common form of diabetes characterised by insulin resistance, which progressively leads to reduced insulin secretion and the development of secondary insulin deficiency (4). Gestational diabetes was historically defined as a degree of glucose intolerance during pregnancy and is diagnosed in the second or third trimester of pregnancy in women without previous history of diabetes (4). Diabetes can occur both in and ex- utero. However, regardless of the type of diabetes mellitus, a common underlying pathological feature is hyperglycaemia, as indicated by elevated blood glucose levels (4).

Uncontrolled diabetes leads to several long-term complications that can manifest in almost every body system, including the renal, cardiovascular, and nervous systems, and it is one of the foremost causes of mortality and has high morbidity worldwide (2,4). Notably, among the deaths in uncontrolled diabetes mellitus, almost one-third to one-half of them are due to

cardiovascular diseases (2). Cardiovascular diseases are a group of disorders affecting the heart and blood vessels and include coronary artery disease, peripheral arterial disease, congenital heart disease, and cardiomyopathy (5). Among these disorders, heart failure mainly results from a structural and electrical maladaptation called pathological cardiac remodelling, which is a deleterious process whereby persistent stress results in poor prognoses like ventricular dysfunction and malignant arrhythmias (6).

1.2 Diabetic cardiac remodelling

In vivo, diabetes is associated with a myriad of manifestations, including altered strain rate, changes in fractional shortening, and modifications to the heart's ventricular wall. Strain-strain rate is the measure of descriptors of the nature and function of cardiac tissue (7). In diabetes, changes to the strain rate manifest as global deformations of the myocardium, as demonstrated by Kaushik et al. (2018) (8). Further, metabolic diseases like diabetes are associated with left ventricular (LV) remodelling and compromised function. These have been demonstrated by Yoneyama et al. (2018), showing that participants from the Multi-Ethnic Study of Atherosclerosis clinical trial with glucose metabolism disorders had LV concentric remodelling, less spherical shape, and reduced systolic myocardial shortening (9). Hyperglycaemia, hyperinsulinemia, and insulin resistance are causative factors contributing to pathological cardiomyocyte remodelling and are thus termed diabetic cardiac remodelling, with hyperglycaemia being a central feature since it is present in all forms of diabetes (10).

Hallmarks of diabetic cardiac remodelling include cardiomyocyte hypertrophy, fibrosis, and apoptosis (11). Initial compensatory mechanisms serve to normalise cardiac function, however, under habitual stress, this mechanism fails – leading to heart failure (11). Physiological cardiac hypertrophy occurs in healthy individuals triggered in response to

pregnancy or physical exercise and is not associated with cardiac damage(12). Pathological hypertrophy occurs due to chronic pressure or volume overload and unlike physiological hypertrophy, there are increases in the foetal gene program, resulting in the re-expression of contractile proteins like myosin heavy chain (MHC), atrial or B-type natriuretic peptides (ANP, BNP), and α-skeletal actin (α-SKA) (13,14). In diabetic cardiac remodelling, cardiac fibrosis and occurs due to pathological alterations of the extracellular matrix (ECM) and can lead to cardiac dysfunction, heart failure, and death (15). Physiologically, the ECM is vital for metabolism, cell proliferation, and motility, however, in pathological conditions like diabetes, changes in the ECM lead to fibrosis resulting in cardiac stiffness and dysfunction(15). These structural changes ultimately lead to apoptosis (16). Chronic diabetes is also associated with Ca^{2+} handling abnormalities, where an excessive amount of intracellular Ca^{2+} produces cell damage, contractile failure, and impaired sensitivity to myofibrils (17,18).

Several factors contribute to the development and progression of cardiac remodelling (19). These factors may have detrimental effects on cardiomyocyte structure and function e.g., cardiac fibrosis alters the contractility and relaxation of cardiomyocytes (19). At a molecular level, pathological stresses induce foetal gene reprogramming, coupled with the downregulation of adult cardiac genes and thus leading to cardiac remodelling and heart failure (20–22). The mechanisms whereby hyperglycaemia contributes to cardiac remodelling have not been fully characterised, however, several metabolic pathways have been proposed to contribute to cardiovascular complications in diabetes (23). These include increased oxidative stress (24,25), chronic inflammation (26), activation of protein kinase C (26), and the production of advanced glycation end products (AGEs). Among these factors, oxidative stress is one of the central mechanisms leading to diabetic cardiovascular diseases since it,

directly and indirectly, contributes to several diabetic pathological pathways (27). Furthermore, it's proposed to be a causative factor contributing to inadequate foetal development and programming of cardiovascular disease (28), vascular alterations, and endothelial dysfunction in animal models of foetal programming (28).

1.3 Role of oxidative stress

Oxidative stress is the disparity in reactive species homeostasis as a result of an imbalance between reactive oxygen/nitrogen species (ROS and RNS) production and their degradation or clearance (29), and this often negatively impacts cellular metabolism (25). ROS are sub-divided into free radicals e.g., superoxide O_2^-; nitric oxide (NO^-); hydroxyl (OH^-) and non-radical by-products produced from O_2 e.g., hydrogen peroxide (H_2O_2) and peroxynitrite ($ONOO^-$) (29). Physiologically, low levels of ROS are essential for redox regulation of physiological signalling and are vital in cell-tissue differentiation and growth (30). Typically, optimal amounts of ROS are produced and act as signalling molecules for regulating transcription factors and apoptotic gene expression (31). Uncontrolled ROS are typically produced as by-products from the mitochondrial electron transport chain during ATP synthesis, referred to as mitochondrial dysfunction (32). In diabetic patients, increased utilisation of mitochondrial fatty acid oxidation and impaired glucose consumption results in compromised mitochondrial functioning and oxidative stress (32). Studies in mice have demonstrated that diabetic hearts exhibited morphological abnormalities, including swollen mitochondria and breakages of the mitochondrial membrane compared to the healthy control hearts (33). Moreover, oxidative stress often results in superoxides directly interacting with protein targets, resulting in oxidation and phosphorylation (post-translation modifications of proteins) (34). Importantly, oxidative stress produces subcellular defects in organelles like the sarcolemma, sarcoplasmic reticulum, and myofibrils (17). These derangements are critical in the pathogenesis of diabetic cardiomyopathy.

Diabetes, hypertension, and obesity are examples of pathological diseases that increase the activation of numerous ROS-producing enzymes. This increased activity leads to excessive ROS levels, thereby overwhelming the endogenous antioxidant-scavenging systems and thus causing a shift in the oxidative-antioxidant balance, favouring oxidation (35).

1.3.2 Enzymatic sources of ROS

Several intracellular producers of ROS have demonstrated susceptibility to diabetes (36). Cytochrome p450, an enzyme localised in the lipid bilayer of hepatocytes and the endoplasmic reticulum, is responsible for the breakdown of xenobiotics i.e., the breakdown of drugs into soluble products, in the process, generating ROS as a by-product (37). In diabetes, however, its expression and activity increase, contributing to increases in ROS (38). During physiological ATP production, 1-5% of all oxygen consumed via oxidative phosphorylation generates superoxides (39). These low levels of mitochondrial ROS are metabolised and detoxified by superoxide dismutase or catalases in the mitochondria/cellular cytoplasm. However, stimulation of cultured cells by high glucose concentrations was demonstrated to increase ROS production (40). This increase in ROS is associated with compromised ATP production and mitochondria regulation, thus promoting mitochondrial dysfunction (41).

Xanthine oxidase (XO) is essential for catalysing the oxidation of the substrates hypoxanthine and xanthine to uric acid. In doing so, this process generates O_2^- and H_2O_2 (39). These reactive species are cleared by the antioxidant enzymes GPx and Zn-SOD, located in the cytoplasm. This pathway is a vital source of ROS production in endothelial cells (42). In cardiomyocytes, it's suggested that the XO pathway has a similar role (42), whereby

inhibition of XO leads to improvements in cardiac and vascular function in a canine model of tachyarrhythmia-prone heart failure (HF) (43).

Nicotinamide adenine dinucleotide phosphate (NADPH) oxidase (NOX) is a family of enzyme complexes, typically found in the membranes of neutrophils and located in organs and tissue throughout the body (44). NOX is a primary contributor to oxidative stress, where there is an uncompensated increase in its activity and hence, elevated ROS production. This increase often leads to DNA damage, deleterious signalling cascades, and host disease states (44). Whereas the other ROS producers have several products, in addition to ROS, the NOX family of enzymes' primary function is to produce ROS, which actively contributes to developmental processes like cardiac development (31). Developmentally, NOX-derived ROS is essential in regulating cell growth and differentiation, with its absence preventing the formation of beating cardiac cells within embryoid bodies and hence, stunting cardiomyocyte formation (45). Moreover, evidence suggests NOX is sensitive to diabetes - exhibiting increased activity and thus elevated superoxide anion formation – resulting in increased cell death and promoting high glucose-induced foetal gene expression (46). However, the contribution of NOX sourced ROS in diabetic-induced oxidative stress remains ambiguous. Several studies have demonstrated in hyperglycaemic conditions, cardiomyocytes have increased NOX2 expression and elevated ROS (47–49). Contrary to these studies, Maalouf et al. (2012) demonstrated that NOX2 activity and expression levels remaining unchanged in the diabetic cardiomyocytes, with NOX4 activity being susceptible to hyperglycaemia (46).

1.4 Protein kinase signalling of ROS

No single theory has been established to explain the signalling pathways implicated in the cardiac pathology induced by hyperglycaemia (50). It is suggested that increased ROS

production due to hyperglycaemia may produce the formation of advanced glycation end products and act via the activation of ROS-sensitive proteins like protein kinases (50). Protein kinases are sensitive to oxidative stress in general, where increased levels of ROS often lead to the activation of downstream effector pathways, including protein kinase C (PKC) (51), phosphatidylinositol-3-phosphate kinase (PI3K)/Akt (PI3K/Akt) (52) and the mitogen-activated protein kinases (MAPKs) (45). Among all these, the mitogen-activated protein kinase (MAPK) appears to be a central effector pathway sensitive to ROS and implicated in cardiogenesis. Li et al. demonstrated that NOX-derived ROS led to increased activation of p38 MAPK in both embryonic stem cells (ESCs) and embryoid bodies (EBs) (45). Nonetheless, the contribution of MAPK in diabetic remodelling is still not fully understood.

1.4.2 Mitogen Activated Protein Kinases (MAPKs)

The mitogen-activated protein kinases (MAPK) are a family of protein kinases essential in relaying biological, extracellular signals from the cell membrane to the nucleus via a series of phosphorylation events (53). Conventionally, MAPKs are composed of a cascade of serine/threonine kinases, starting with MAPK kinase kinase, MAPK kinase, and MAPK, eventually ending with the dual phosphorylation of MAPK on serine and tyrosine (54). There are four common MAPK signalling cascades, namely the extracellular signal-regulated kinases (ERK 1/2), c-Jun N terminal kinases (Jnk 1, 2, 3), ERK 5, and the p38 MAPK (53). Of these, the p38 MAPK and Jnk are typically activated in response to environmental stresses and inflammatory stimuli like oxidant stress, infections, and cytokines (55), and are thus collectively known as stress-activated protein kinases (SAPKs).

p38 MAPK in cardiac remodelling

The p38 MAPK family consists of four isoforms; p38α, p38β, p38γ, and p38δ. p38α and β are ubiquitously expressed and have approximately a 74% structural homology. p38γ and δ, however, are less characterised and expressed – with the expression of these isoforms detected in skeletal and cardiac muscle (γ) and lungs, spleen, and testis (δ) (56). These isoforms are less homologous than the α isoform, with only 60% similarity (57,58). p38 MAPK is activated by the dual phosphorylation of residues upstream of MKKs, which subsequently activate MKK kinases thus forming the canonical activation signalling pathway (57). The p38 activation loop consists of a TGY motif, with the tyrosine (Y) and threonine (T) residues being phospho-activators within the activation loop. When inactivated, the substrate binding channel is blocked by the activation loop. Dual phosphorylation of TGY at tyrosine and threonine within the activation loop causes a conformational change, in doing so, exposing the substrate binding channel (57).

p38 MAPK is pivotal in regulating cardiac development and remodelling. p38α is the most well-characterised and studied isoform. Developmentally, knockout of it leads to lethality in embryos' whereas knockout of the other isoforms (β, δ, γ) results in a near-normal phenotype (59–61). Additionally, a study by Li et al. demonstrated that inhibition of p38 MAPK substantially reduced the amount of beating cells *in vitro*, and the expression of myocyte enhancer factor 2C (MEF2C), a crucial transcription factor implicated in the activation of several cardiac-specific embryonic genes and hence promoting cardiovascular development (62,63). However, several investigations demonstrate the activation of p38 MAPK in pathological conditions leads to pathological cardiac remodelling which progresses to heart failure (HF) (64). HF comprises several abnormalities in the heart muscle, pericardium, and

valves – along with disturbances in cytokine and ventricular function (65). Such abnormalities often result from contractile alterations, hypertrophy, fibrosis, apoptosis, and inflammatory cytokines and are hallmarks of cardiac remodelling (66). p38 MAPK activation has been documented to show reduced contractility and enhanced matrix remodelling (67). Additionally, activation of the p38 MAPK pathway via gene transfer of kinases upstream of p38 MAPK i.e., MKK 3/6, or the inhibition of the pathway via a p38 MAPK negative mutant, results in adverse changes in contractility in the heart (68). Similarly, in cultured cardiomyocytes, inhibition of p38 MAPK activation attenuates hypertrophy induced by endothelial and phenylephrine stimulation (69). Hoefer et al. demonstrated the activation of p38 MAPK in vessel walls in response to stresses like hypoxia and pressure overload (70). Furthermore, *in vivo* rat models of heart failure demonstrated that inhibition of p38 MAPK, with SB239063, prevented endothelial dysfunction and normalised ventricular p38 MAPK activity (71) by reducing superoxide anion generation – thus implicating p38 MAPK in ROS generation during heart failure (71).

Apoptosis is one of the three cell death systems regulated by several stress-activated signalling pathways. p38 MAPK is one such pathway, however, the overall outcome of the role of p38 MAPK in a cardiac setting remain ambiguous. Depending on the cell type and stimuli, it can have both pro- and anti-apoptotic effects (66,72). Several studies have tried to elucidate the role of p38 MAPK in apoptosis, however, findings remain contradictory. Thandavarayan et al. (2009) suggest that p38 MAPK is pro-apoptotic. This study showed that diabetic transgenic mice, overexpressing dominant negative p38α had attenuated levels of myocardial apoptosis, caspase-3 positive cells, and the downregulation of anti-apoptotic proteins like B-cell lymphoma extra-large (Bcl-x) (73). Although evidence suggests p38α drives apoptosis in diabetes-induced cardiomyocytes, other studies have demonstrated p38β

may be implicated in anti-apoptotic outcomes and increasing protein synthesis in diabetes (74,75).

While numerous studies have investigated the role of p38 MAPK in diabetic cardiomyopathy, most of these were performed using animal models or terminally differentiated cardiac tissue. This impedes our overall understanding of remodelling, and given that pathological remodelling results in the re-expression of foetal genes to cater to the increased stress, it further impedes our understanding of the pathology involved in cardiac remodelling (13,14).

Given that p38 MAPK is implicated in both cardiac development and the pathogenesis of diabetic cardiomyopathy, an understanding of the modulation of the p38MAPK signalling pathway and its possible involvement in the shift from physiological to pathological outcomes in diabetic hearts is needed (particularly in a developmental model). Further, most studies investigated the role of the dominant isoforms i.e., p38α – as such, the precise role of lowly expressed isoforms is still largely unknown. Understanding the involvement of p38 MAPK in diabetic cardiomyocytes (in a developmental model) may provide us with alternative therapeutic targets for treating diabetic cardiomyopathy.

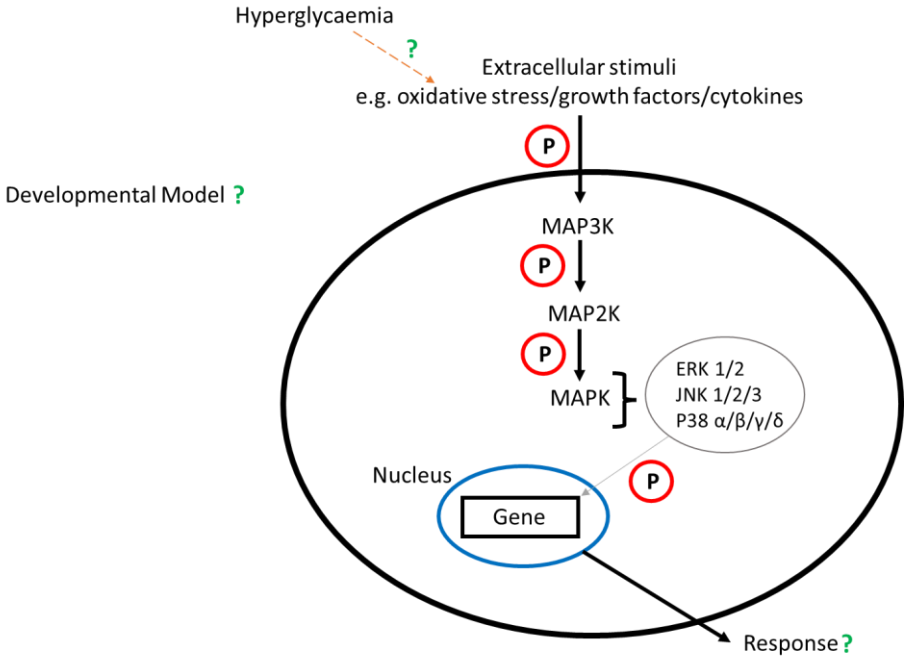

Figure 1: Implication of p38 MAPK signalling pathway in the diabetic heart. *Simplified representation of the classical MAPK signalling pathway in mammalian tissue. MAPK consists of three kinases that activate and phosphorylate (indicated by the letter P) one another. MAPK pathway activation is stimulated by cellular stress, growth factors, and cytokine stimulation. Activation of MAPK regulates downstream substrates in the nucleus e.g., transcription factors. MAPK3K – Mitogen-activated protein kinase kinase kinase.*

2. Aims and Objectives

2.1 Aim

To study the effect of hyperglycaemia-induced oxidative stress and the possible involvement of the p38 MAPK pathway in cardiac remodelling during cardiac development.

2.2 Hypothesis

In a developmental model, hyperglycaemia detrimentally affects our cells by stimulating the p38 MAPK signalling pathway via an increase in oxidative stress.

2.3 Specific Objectives:

(a) To establish a mild-moderate oxidative stress cardiac cellular model

(b) To evaluate the effect of hyperglycaemia and oxidative stress on cardiac-like cells

(c) To explore the possible involvement of the p38 MAPK signalling pathway

2.4 Novelty of the Research

p38 MAPK and ROS have previously been demonstrated to be vital for cardiogenesis, however, strong evidence also suggests an increase in both leads to several pathological outcomes including apoptosis, inflammation, and hypertrophy. This study assessed the role of p38 MAPK and its crosstalk with hyperglycaemia-induced oxidative stress. Understanding the role of p38 MAPK in hyperglycaemia-induced cardiac remodelling, particularly in a developmental model, may provide us with novel therapeutic targets to manage disease pathology.

3. Methods

3.1 Cell Culture

Pluripotent mouse embryonic stem cells (mESCs; cell line BALB/c ES129 OLA) were used in this study (provided by Professor Frank Brombacher from the University of Cape Town, SA). Cell lines were cultured in 6-well culture plates (35mm well) under standard culture conditions (5% CO_2, 37°C, 95% humidity). Cell culture reagents were purchased from Thermo-Fischer Scientific (LTC Tech, SA) unless otherwise stated.

This study uses cardiac-like cells and hyperglycaemia as an *in vitro* model of the diabetic heart, allowing us to identify and evaluate signalling mechanisms that occur in specific cells during the remodelling process. Using mESCs to generate cardiac-like cells is particularly useful when studying remodelling, *in vitro*, compared to using other cell lines (immortal cardiac cell lines) due to the expression of several cardiac-specific markers like α-actin and desmin (76,77). As mESCs mature, they aggregate or cluster to form 3D structures called embryonic bodies (EBs) (78). Within these EB aggregates, there're spontaneously beating regions, which are functional properties of cardiomyocytes. Unlike most *in vitro* models, these beating foci allow us to characterise functional, structural, and molecular alterations. EBs are heterogenous and form derivatives of all three germ layers, namely the ectoderm, mesoderm, and endoderm - making this model physiologically relevant. Additionally, this model allows us to characterise the same cells at several time points.

3.1.2 Pluripotent mESC proliferation

mESCs were grown on a feeder layer of inactivated mouse embryonic fibroblasts (iMEFS). Mouse embryonic fibroblasts from American Type Culture Collection (ATCC) were inactivated with mitomycin C (1mg/ml) – thereby keeping cells in their metabolically active

state whilst preventing replication (**Appendix A1**). In doing so, the feeder cells support the growth of cells with low clonal density by 1) acting as a substrate for cell attachment, (79) 2) detoxifying growth media (79), and 3) synthesizing and secreting cytokines into the culture medium (80).

iMEFs, stored in liquid nitrogen, were gradually thawed in a 37°C water bath and transferred to a centrifuge tube containing pre-warmed medium – this is essential to support the survival of cells by diluting out DMSO from the freezing medium. Cells were pelleted by centrifugation for 5 minutes at 1500rpm. The supernatant was aspirated, and the cell pellet was resuspended in a growth medium consisting of 4.5g/l DMEM (supplemented with 10% Heat-inactivate (HI) FBS; 1% glutamax; 1% penicillin/streptomycin; 0.1% β-mercaptoethanol). The cell suspension was split over two 0.1% gelatin (w/v) coated wells, seeding 150 000 cells/well. Cells were incubated for 24-48 hours under standard culture conditions. Two hours before mESC seeding, the growth medium was removed and replaced with ES medium, 4.5g/l DMEM (supplemented with 10% HI-FBS; 1% glutamax; 1% penicillin/streptomycin; 0.1% β-mercaptoethanol and 5ng/ml Leukaemia inhibitory factor (LIF; #A35933, ThermoScientific). mESCs were thawed and pelleted by centrifugation before resuspending in ES medium and subsequent seeding on feeder layers. mESCs on feeder cells were incubated for 48 hours or until ≈50-60% confluency under standard culture conditions. The medium was replenished every 48 hours. At a confluency of ≈50%, mESCs were enzymatically detached from the feeder layer using dispase II protease solution (5mg/ml; Sigma, SA) for 15-20 minutes under standard culture conditions. Following detachment, enzyme activity was inactivated with media containing 10% heat-inactivated foetal bovine serum (HI-FBS) and transferred to a centrifuge tube. Cells were pelleted, and the supernatant was removed before resuspending in fresh ES medium. The cell suspension was split over two pre-prepared wells containing feeder layers. Cells were passaged 2-3 times

before proceeding with differentiation protocol – this is essential to ensure mESCs have maintained pluripotency and not spontaneously differentiating. Contamination of cells is an issue when performing cell culture, with mycoplasma being one of the most detrimental due to this organism being resistant to most antibiotics. mESCs were routinely tested for mycoplasma, to confirm we are working with uncontaminated cultures (**Appendix A2**).

3.1.3 Cardiac differentiation

The mESCs were differentiated into stem cell-derived cardiac-like cells by forming embryoid bodies (EBs) using the hanging drop method as described by Aboalgasm et al. (81,82) (**Figure 2**). Briefly, confluent mESCs (70-80%) were dissociated from the iMEF feeder layer using the protease dispase II (5mg/ml). Cells were counted using a haemocytometer. A fixed number of cells were seeded into each hanging drop (20µl) of differentiation medium; consisting of 4.5g/l or 25mM DMEM (supplemented with 10% HI-FBS; 1% glutamax; 1% penicillin/streptomycin; 0.1% β-mercaptoethanol). Seeding a fixed number of cells per drop, we were able to control EB size and, at the same time, maximise functional activity, allowing for more reproducible and homogenous EBs (81,83). The first day of the hanging drop protocol was considered day 0 of differentiation. Droplets were incubated and left undisturbed for three days under standard culture conditions, allowing for stem cell aggregation and EB assembly. The rounded bottom of the hanging drops allowed for the self the aggregation of mESCs, using only gravity as an aggregating factor, thus providing a suitable environment for EB formation without introducing additional confounding elements. (**Figure 2A**).

EBs were transferred to a 10cm bacteriological dish for suspension culture for four days, allowing EBs to grow (**Figure 2A**) before being seeded on 0.1% gelatin-coated culture plates for further culturing (day 7 of differentiation). EBs were cultured and maintained in 25mM

media and replenished every 2-3 days (**Figure 2A**). Following the appearance of pulsatile foci, EBs were subjected to respective interventions, and analysis was performed (**Figure 2B**).

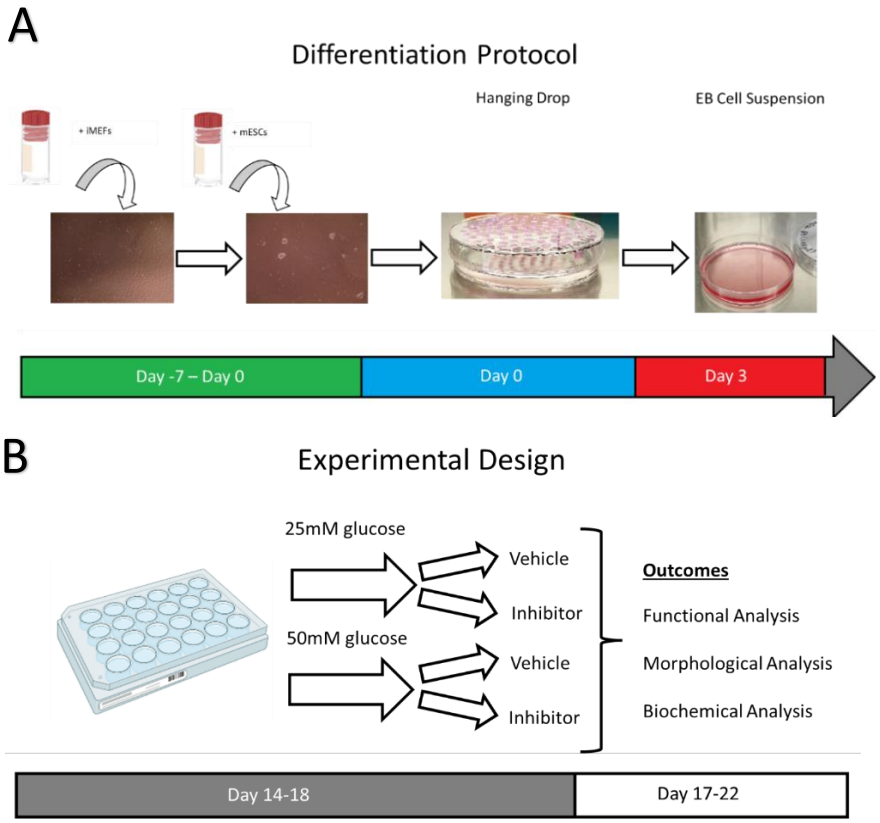

Figure 2: Schematic depicting the differentiation protocol and experimental design for the formation of cardiomyocytes from mESCs. ***A)****129 OLA mESCs are expanded on feeder layers of iMEFs until 70-80% confluency. mESCs in the differentiation medium undergo self-aggregation using the hanging drop method (Day 0). EB transfer to a cell suspension for further differentiation (Day 3). On day 7 of the differentiation protocol, EBs were transferred to 0.1% gelatin-coated cell culture plates for further differentiation.* ***B)*** *Pulsatile cardiac-like EBs between days 14 and 18 were subjected to treatment, followed by functional, morphological analysis, and cell harvesting.*

Differentiating mESCs into cardiac-like EBs is dependent on the number of cells seeded per hanging drop. To determine the optimal number of cells, 500 and 1000 mESCs were seeded per hanging drop. We found that the pattern in which EB grew and started to beat remained consistent, irrespective of the number of cells seeded per drop (**Appendix A5**). Given that

seeding 1000 cells/drop had a slightly higher EB yield compared to 500 cells/drop, and it has previously been used in other studies (82), this concentration was used as a default for all subsequent experiments. Given the nature of the growth pattern, pulsatile EBs selected for treatments were between days 14 and 18 – where most EBs began exhibiting beating activity (**Appendix A5**).

Changes in cell morphology and functional activity were observed by light microscopy, using EVOs XL Core microscope. Images were captured from the same wells at several time points to detect changes in morphology over time. Images were captured at 2x or 4x magnification (EVOs XL Core). Using ImageJ software, EB diameter was measured by taking an average of four measurements per sample (vertical, horizontal, and two diagonal) (**Figure 3B**). For better visualization of the EBs, the 'Find Edges' function on ImageJ was used - allowing for better visualization of the less densely populated area of cells, particularly those on the periphery. Functional changes like the beating efficiency and the beating rates were measured. Beating efficiency was evaluated as the percentage of beating EBs (Number of beatings EBs relative to total EBs x 100). Beating rates were measured by counting the number of contractions over a 30-second interval to determine beats per minute (BPM).

The typical outcome of the differentiation protocol manifested as non-adherent EBs in suspension culture on day 5 (**Figure 3A**). By day 10 the EBs were adherent on the coverslips and started exhibiting spontaneously beating foci (**Figure 3B**). The pulsatile cardiac-like EBs had fully matured (**Figure 3D**) and exhibited a positive expression for the cytoskeletal f-actin filament marker, phalloidin (**Figure 3C**) as seen in previous studies (84).

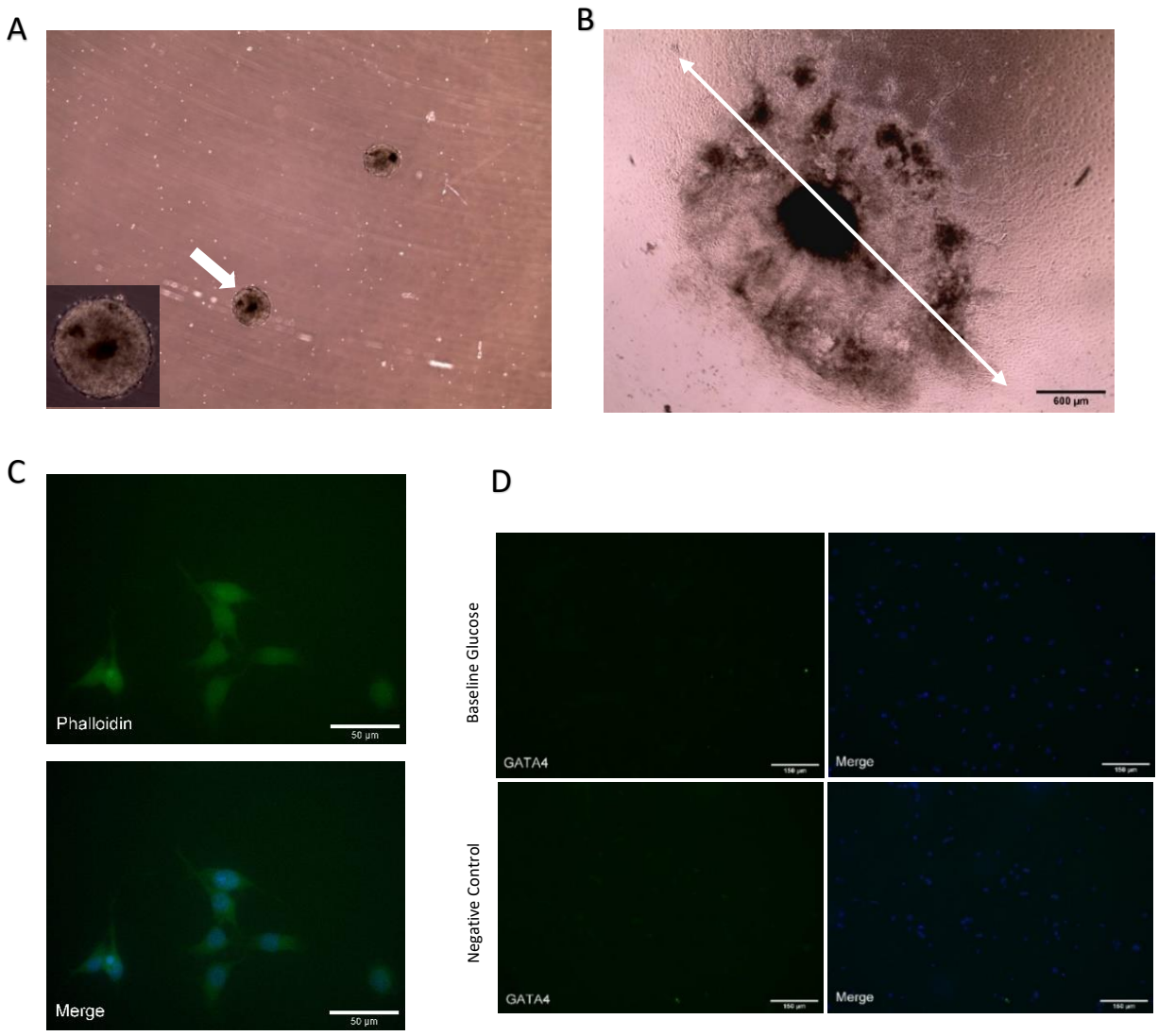

Figure 3: Typical stem-cell derived cardiac-like EB phenotype. ***A)*** *Representative Light microscopy image of Embryoid body in suspension on day 5 of differentiation protocol (inset 10x)* ***B)*** *Light microscopy image of pulsatile cardiac-like cells at day 11 (4x) with the diagonal line indicating diameter Scale=150µm.* ***C)*** *Representative immunofluorescent image of phalloidin (green) in cardiac-like EBs (40x) scale=50µm.* ***D)*** *Representative immunofluorescent images of GATA4 (Green) to exhibit gene expression in stem cell-derived cardiac-like cells, nuclei stained with Hoechst (Blue), and merged images (10x) (n=2 independent culture batches, with n=3 EBs).*

3.1.4 Experimental Design and Treatments

Pulsatile EBs were treated with baseline glucose (25mM) or an adequate dose of high glucose (50mM) to induce oxidative stress for 72 hours under standard culture conditions. A 72-hour exposure with hyperglycaemia was used in previous *in vitro* culture systems of erythrocytes

and cardiac fibroblasts (85,86). Even though 25mM is considered supraphysiological, it is the default glucose concentration used to culture mESCs *in vitro* during cardiomyocyte differentiation (82,87,88). This concentration has been shown to promote cardiomyocyte differentiation by producing controlled amounts of beneficial ROS (89). To mimic hyperglycaemia, a concentration of 50mM glucose was used, similar to hyperglycaemic models of cardiac-like H9C2 cells and 129 OLA mESCs (82,90,91). Other studies have used 5.5mM glucose as normoglycaemia in vitro. However, given that the mESCs were grown and maintained at 25mM glucose, reducing concentrations to 5.5mM, there is a risk of starving cells of nutrients essential for survival. Changes in osmolality from glucose were not corrected, enabling us to imitate physiological diabetic conditions, where hyperglycaemia is inherently coupled with changes in osmolality.

To verify the presence of oxidative stress, a known pro-oxidant, hydrogen peroxide (100μM) was also used. To determine the optimal dose of hydrogen peroxide required to cause mild-moderate levels of oxidative stress, cardiac-like EBs were subjected to concentrations of 0, 100, or 1000μm hydrogen peroxide (H_2O_2). Treatment with 1mM hydrogen peroxide in 25mM media caused the EBs to lose adherence and resulted in significant cellular disruptions and cessation in their pulsatile activity (n=3) (**Figure 4**). EBs treated with 100μM-hydrogen peroxide remained adherent, maintained beating activity, and showed no gross morphological changes (**Figure 4**). Treatment with hydrogen peroxide (100μM) was thus used as an oxidative stress control as it wasn't lethal during an acute insult and allowed us to characterise beating characteristics. To validate the degree of oxidative stress produced by 100μM hydrogen peroxide and our proposed high glucose concentration (50mM) was mild-moderate, we probed for nitrotyrosine, a marker of ROS-induced permanent protein damage.

Results indicated that nitrotyrosine is undetected in baseline, high glucose, and hydrogen peroxide treated groups, suggesting that the oxidative stress induced is mild.

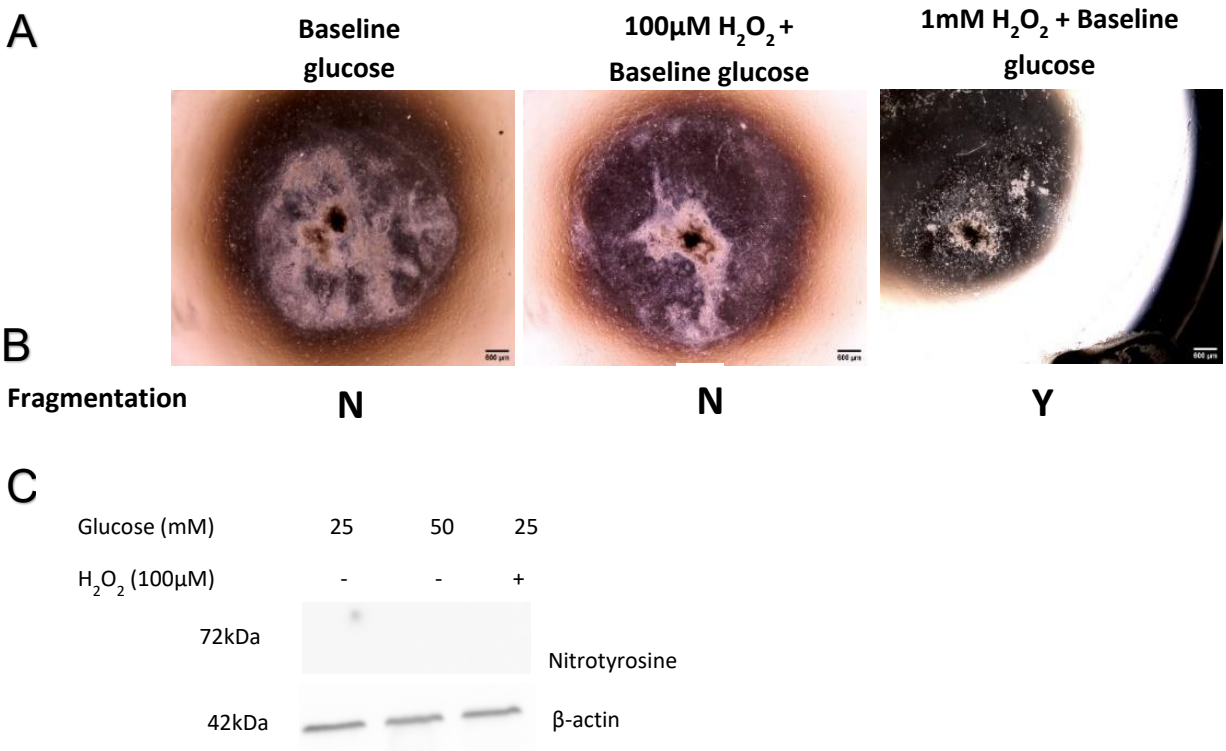

Figure 4: EB sensitivity to oxidative stress. ***A)*** *Representative light-microscopy images showing the effect of different concentrations of hydrogen peroxide on pulsatile mESC-derived cardiac-like EBs. EBs were subjected to 0µM, 100µM, or 1mM hydrogen peroxide in baseline conditions (2x magnification) (n≥3 EBs per group). Scale=600µm.* ***B)*** *Qualitative analysis representing fragmentation "Y" indicating fragmentation and "N" indicating no fragmentation (n=3 EBs per group).* ***C)*** *Representative western blot of nitrotyrosine (protein damage marker), and β-actin, set as control (n=3).*

Diphenyleneiodonium chloride (DPI; CAS 4673-26-1; Merck Life Science) was used to inhibit NADPH oxidase and SB203580 (CAS 152121-47-6; Merck Life Science) for the inhibition of p38 MAPK. Stock compounds of DPI and SB203580 were dissolved in dimethyl sulfoxide (DMSO; Sigma-Aldrich) and used at concentrations of 2µM and 5µM respectively. These concentrations were used in previous studies and shown to effectively inhibit their respective targets (45). An equivalent volume of the vehicle (DMSO), present in the experimental samples, was added to controls in each experiment. The final concentration

of the vehicle in the culture was less than 0.01%. Pulsatile mESC-derived cardiac-like EBs were pre-incubated with glucose (25mM) medium and supplemented with the inhibitors tested (DPI or SB203580) for 1 hour - this is essential for conditioning cells to the inhibitor.

3.2 Immunocytochemistry

Adherent mESC-derived cardiac-like EBs were stained post-treatment. Embryoid bodies are three-dimensional structures composed of several overlaying cells - making it difficult to observe individual cells and quantification of total cell numbers difficult. For this reason, cells were stained in whole EBs, or EBs were enzymatically digested to generate adherent monolayers and subsequently stained. Briefly, cells were washed three times with 1xPBS, followed by a 15-minute fixation with 4% (w/v) paraformaldehyde (PFA) in PBS at room temperature (92). Excess PFA was removed by rinsing cells thrice with ice-cold 1xPBS before permeabilizing with ice-cold methanol for 15 minutes at room temperature. To prevent non-specific binding of antibodies, samples were blocked with blocking buffer (3% BSA (w/v), 0.01% Triton-X (v/v) in 1xPBS) for 2 hours at room temperature, followed by overnight incubation at 4°C with the primary antibody the polyclonal antibody, or 1-hour incubation at room temperature with the stain Phalloidin (1:5000) diluted in 1% BSA (w/v). Following labelling of the protein of interest, the unbound primary antibody was washed away, and samples were incubated in the dark with conjugated secondary antibody for 2 hours at room temperature – secondary antibody addition was not required for direct stains. Cells were counterstained with the nuclear stain Hoechst 3325 (0.5µg/mL; Sigma, SA) for 10 minutes in the dark and at room temperature before mounting onto microscope slides using mowiol mounting solution supplemented with antifade. Slides were air-dried overnight before being stored at 4°C. Slides were imaged using EVOs M5000 (ThermoScientific), and analysis was performed using ImageJ software.

For the digestion of EBs, following treatment, the medium was removed, and the cardiac-like EBs were lifted and dissociated in Trypsin/EDTA (T/E) (0.5g/l Trypsin/0.2g/l EDTA, pH 7.4) for 20 minutes under standard culture conditions. Lifted cells were gently triturated four times in T/E followed by enzyme inactivation with media containing FBS. Cells were pelleted by centrifugation and the supernatant was removed. The cell pellet was resuspended in fresh medium, followed by reseeding on a 0.1% gelatin-coated 35mm culture dish for 16-24 hours under standard culture conditions to allow for sufficient cell adherence, without cell clusters forming (**Appendix A6**). Adherent cells were subsequently fixed and stained with a primary antibody against GATA4 (GATA4; dilution 1:1000; Cat#pa5-29663, ThermoScientific) followed by incubation with Alexa Fluor 488(dilution 1:500; Cat#715-546-150, Amersham) secondary antibody or stained with propidium iodide followed by cell imaging.

For live cell imaging, adherent cells were stained with propidium iodide (1mg/ml) (PI; Cat #P4170; Sigma-Aldrich), a nuclear stain integrated into dead or compromised cells, and Hoechst 3325 (10µg/µl), a non-specific nuclear stain. Briefly, media was aspirated, and cells were washed with 1xPBS followed by staining with PI (1:5000) and Hoechst (1:5000) in 1xPBS for 10 minutes at room temperature and in the dark. The staining solution was removed, and cells were rinsed with 1xPBS, followed by immediate fluorescence microscopy (EVOS M5000). Three images were captured per EB and analysed using ImageJ software, determining the proportion of PI-positive nuclei relative to total nuclei.

3.2.2 EdU assay

Cell proliferation of adherent cells was determined using an EdU incorporation assay. The detection of the thymidine analogue, EdU, into newly synthesized DNA was performed by immunofluorescent staining, using the Click-iT EdU Imaging assay kit (C#10337, Thermoscientific), according to the manufacturer's specifications. Briefly, EBs were digested and reseeded on 0.1% gelatin-coated coverslips post-treatment for 16-24 hours followed by incubating under standard culture conditions with 10μM EdU stock solution in a pre-warmed culture medium for 6 hours (93). The labelling solution was removed, and cells were fixed with 4% PFA in PBS for 15 minutes, followed by permeabilization with 0.5% Triton-X 100 in PBS for 20 minutes. ClickiT^{TM} reaction cocktail solution was made as required on the day of the assay. The sample was incubated in 400μl (per sample) of reaction cocktail and gently agitated for 2 minutes, allowing for even distribution – followed by a 30-minute incubation at room temperature in the dark (93). The samples were counterstained with Hoechst 3325 (0.5μg/ml) before being imaged by fluorescent microscopy (EVOS M5000). Images were analysed using ImageJ software, determining the proportion of EdU-stained nuclei relative to total nuclei.

3.3 Western blotting

Protein was harvested from EBs seeded in 12 and 24 well plates. Cells were washed twice with ice-cold 1xPBS, pH7.5 to remove residual media and treated with cold Radioimmunoprecipitation (RIPA) lysis buffer, consisting of 50mM Tris-HCl (pH 8), 1% Triton x-100, 150mM NaCl, 0.1% sodium dodecyl sulfate (SDS), 0.5% sodium deoxycholate with a protease and phosphatase cocktail inhibitor (Halt protease and phosphatase inhibitor, ThermoScientific, USA). Cells were gently scrubbed from the surface of the plate and mixed in the lysis buffer. Cell lysates were transferred to pre-cooled tubes on ice, with one sample

consisting of 7-10 EBs. Pre-cooling Eppendorf's and keeping samples on ice is essential in preventing the degradation of proteins, especially lowly expressed proteins like phosphorylated proteins. Lysates were briefly vortexed and gently mixed on a roller for 30 minutes at 4°C; followed by centrifugation at 15000 relative centrifugal force for 30 minutes at 4°C (Labnet International, NJ07095, USA). Supernatants were transferred to clean 1.5ml Eppendorf tubes and pellets were discarded. The supernatant was stored at -20°C for long-term storage.

Protein quantification of supernatants was determined using the BCA assay (Pierce BCA protein assay kit) (ThermoScientific, Rockford, USA) - a colorimetric assay where in the presence of proteins, copper ions chelate **(Appendix A TABLE 2**). 10µl of sample supernatant was diluted with RIPA buffer (1:6 dilution ratio) and 25µl of protein samples were loaded in duplicate in a 96-well, flat-bottomed plate. 200µl of BCA working reagent was added to all standard and sample wells, and the plate was covered with parafilm to prevent sample evaporation. Samples were incubated at 37°C for 30 minutes. The absorbance was measured at 560nm using a microplate reader (RT-2100C microplate reader, Rayto). A standard curve was constructed according to the absorbance values of the protein standards, and sample concentrations were calculated using the curve.

30µg/well of homogenised EBs (days 17-22) were prepared in RIPA buffer, followed by the addition of protein loading dye and DTT. Samples were boiled at 95°C for 5 minutes. Prepared samples were subsequently spun down and cooled on ice. Proteins were resolved on 10% SDS polyacrylamide gels. 20µl of samples were loaded, alongside 2µl of protein molecular weight marker (Pageruler prestained protein ladder, #26616, ThermoScientific). Samples were electrophoresed for 40-60 minutes at 150mV (Mini-PROTEAN® Tetra Cell, BioRad, SA).

Proteins on SDS-page gels were transferred and immobilized on a PVDF membrane (Immuno-Blot PVDF Membrane for Protein Blotting, Bio-Rad, SA) using a semi-dry transfer system (Trans-Blot Turbo Transfer System, Bio-Rad, SA). Before protein transfer, two stacks of filter paper (6 filters per stack) were soaked in the transfer buffer. PVDF membranes were activated by soaking in methanol for 1 minute, followed by a brief soak in deionised H_2O, and subsequently equilibrated by soaking in transfer buffer. The proteins were transferred to the PVDF membrane using the Trans-Blot Turbo Transfer System at 25V, 1.3A for 7 minutes at room temperature. Protein transfer efficacy was evaluated by performing a Ponceau S stain (**Appendix A6**).

To prevent nonspecific binding of antibodies during incubation steps, the PVDF membranes were blocked in filtered (to reduce the risk of particulates binding to the membrane) 5% non-fat milk or 5% BSA in PBS-T (Blocking Buffer - 0.1% v/v Tween 20; 1xPBS; 5% w/v non-fat dry milk/ 5% w/v BSA) for 1 hour at room temperature. A primary constituent of milk is casein, a highly abundant protein that may result in a high background when used to block the PVDF membrane, thus masking the detection of low-expressed proteins. For this reason, an alternative blocking agent, Bovine serum albumin (BSA), was used to block and dilute antibodies – when probing for phosphorylated proteins and their total protein counterparts (94,95).

The membranes were incubated with epitope-specific primary antibodies, diluted in 5%BSA or 5% non-fat milk in PBST (**Table 1**); overnight at 4°C under constant agitation. The membranes were then washed thrice for 10 minutes with PBS-T followed by incubation with species-specific secondary antibodies. Membranes were incubated with secondary goat-anti-mouse horseradish peroxidase (HRP) conjugated antibody (1:8000 dilution; Cat#G-21040; ThermoScientific) in the blocking buffer for 2 hours at room temperature.

Proteins were visualised with enhanced chemiluminescent solutions (ECL) containing peroxidase substrates (Clarity Western ECL Substrate, Cat #170-5060, Bio-Rad, SA). Equal volumes of the solutions from the Clarity Western ECL Substrate kit were mixed on the day of detection. Labelled membranes were incubated at room temperature with ECL for 5 minutes, and excess ECL was drained. Membranes were wrapped in a transparency film and exposed to X-ray films (CL-XPosure^{TM} Film, Cat #34090, ThermoScientific, Rockford, USA) for the detection of protein bands.

Captured western blot results were digitized by scanning developed X-ray films as 600 dots per inch (dpi) images. Individual protein bands were measured using ImageJ software, resulting in one profile per signal. Signals with higher intensity resulted in higher and wider peaks. To account for background signals, a line was drawn under each peak thus excluding the underlying area from the measurements. Measured areas are given as arbitrary units and are only comparable in individual blots.

Table 1: Primary antibodies used in this study

Antibody and specificity	**Catalogue number and Supplier**	**Dilution**
β-actin (Monoclonal anti-b-actin antibody produced in mouse)	MA5-15739-1MG; ThermoScientific	1:5000
Nitrotyrosine (Monoclonal anti-nitrotyrosine antibody produced in mouse)	HM11; ThermoScientific	1:250

p38 MAPK (Monoclonal anti p38 MAPK antibody produced in mouse)	p38-3F11; ThermoScientific	1:1000
pp38MAPK (Monoclonal anti-phospho-p38 MAPK antibody produced in mouse)	MA515218; ThermoScientific	1:2000
OPA1 (Monoclonal anti-OPA1 antibody, produced in mouse)	MA516149; ThermoScientific	1:1000

3.4 Statistical Analysis

Values are represented as means ± standard deviation, or as box-and-whisker plots. Statistical analysis was performed using GraphPad Prism version 5.00 software for Windows (GraphPad Software, San Diego USA). A Shapiro-Wilk test for normality was used to determine the distribution of variables. For non-parametric data, Kruskal-Wallis with Dunn's post-test was used. For parametric data, One-Way ANOVA with Tukey's post-test was used with significant $P \leq 0.05$.

4. Results

4.1 Effect of oxidative stress on cardiac-like EB size and cell survival

To investigate the role of hyperglycaemic-induced oxidative stress on stem cell-derived cardiac-like cells, pulsatile EBs were treated in basal (25mM), high (50mM) glucose, or hydrogen peroxide (100µM) in basal glucose. Our data indicated that EBs treated with hydrogen peroxide showed a significant reduction in EB diameter ($p=0.0305$). Treatment with high glucose showed an insignificant change in EB diameter compared to baseline conditions ($p=0.118$), moreover, there was also no change compared to the hydrogen peroxide-treated group ($p=0.8966$) (**Figure 5D**). Functionally EBs maintained beating activity irrespective of glucose concentration or hydrogen peroxide treatment. No noticeable change in beating rate was observed, with baseline being -5.45±42.3%, high glucose 9.85±39.8%, and hydrogen peroxide 14.9±79.6% with no statistical change across all groups (**Appendix B3**).

Given the change in EB diameter when challenged with hydrogen peroxide, the effect of oxidative stress was further investigated by performing a cell viability assay by staining with propidium iodide (PI) and Hoechst. Qualitatively, results demonstrate that hydrogen peroxide resulted in a noticeably higher degree of PI uptake while high glucose resembled the amount of PI seen in baseline treatment (**Figure 5A**). Quantitative analysis revealed that hydrogen peroxide treatment had significantly higher PI uptake versus baseline treatment ($p=0.0019$). These data also showed that high glucose showed no change in PI-positive cells compared to baseline ($p=0.2007$) (**Figure 5B**). Quantification of the number of pyknotic-like nuclei showed a significant increase when subjected to high glucose compared to normal glucose ($p=0.0099$), whereas hydrogen peroxide showed no statistical difference compared to baseline ($p=0.1002$) (**Figure 5C**).

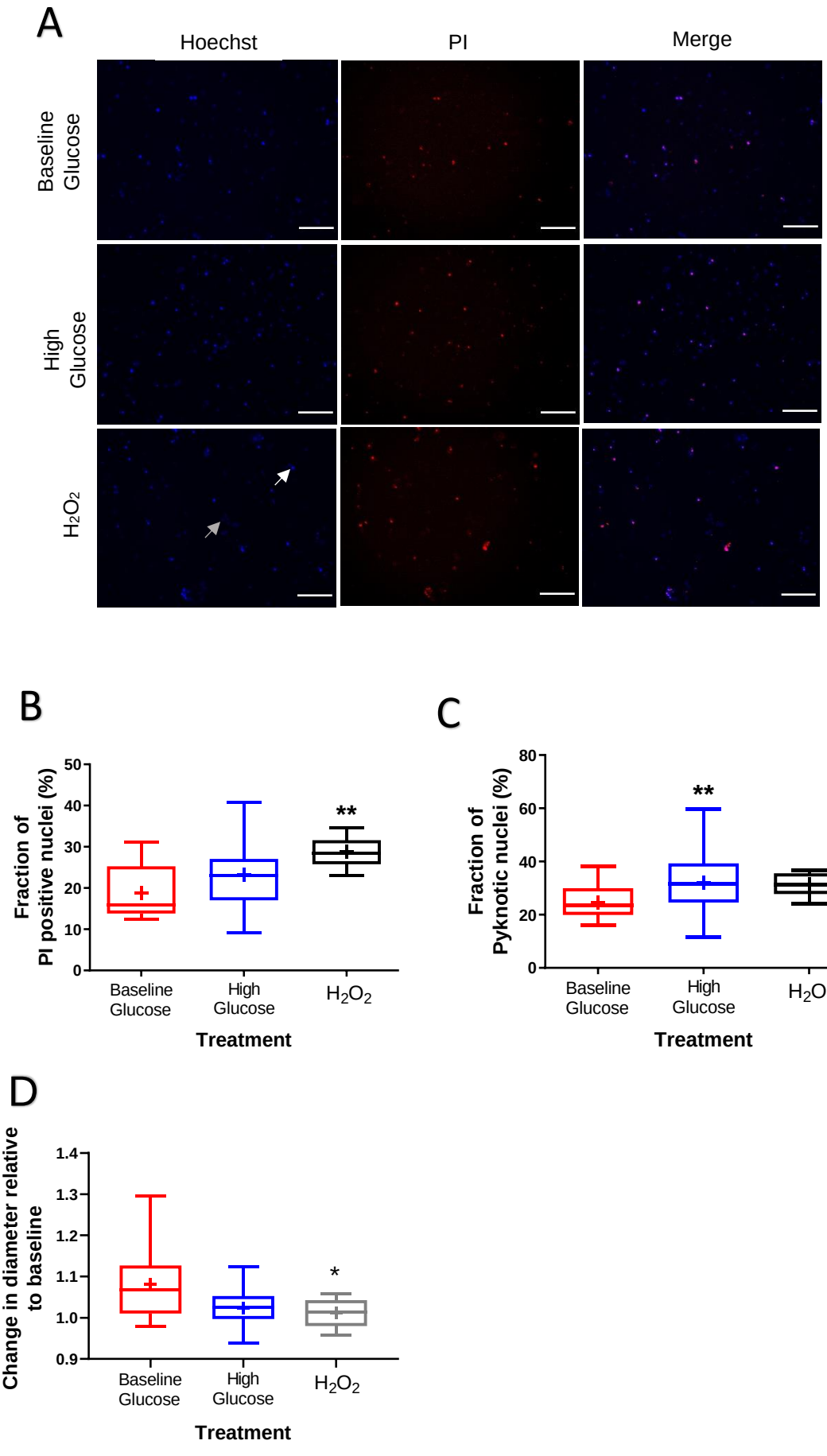
A
Hoechst
PI
Merge
Baseline Glucose
High Glucose
H2O2
B
Fraction of PI positive nuclei (%)
50
40
30
20
10
0
**
Baseline Glucose
High Glucose
H2O2
Treatment
C
Fraction of Pyknotic nuclei (%)
80
60
40
20
0
**
Baseline Glucose
High Glucose
H2O2
Treatment
D
Change in diameter relative to baseline
1.4
1.3
1.2
1.1
1.0
0.9
*
Baseline Glucose
High Glucose
H2O2
Treatment

Figure 5: Effect of oxidative stress on pulsatile mESC-derived cardiac-like EBs. ***A)*** *Representative fluorescence microscopy images of Hoechst (Blue), Propidium iodide (Red), and merged images (10x) with arrowhead indicating pyknosis (white) and normal nuclei morphology (grey). Scale bar = 150µm.* ***B)*** *Quantitative analysis of the %PI positive cells relative to total* ***C)*** *Quantitative analysis of % Pyknotic-like nuclei relative to total (n=3 independent culture batches, n=3-8 EBs per group).* ***D)*** *Quantitative analysis of the change in EB diameter relative to baseline (n=3 independent cell culture batches, n=10-12 EBs per group). B-D) Data represented as a box-and-whisker plot, with mean represented as "+" with significant (*P≤0.05, **P≤0.01) compared to baseline glucose.*

4.2 Effect of NADPH oxidase inhibition on mESC-derived cardiac-like EBs

To investigate a potential source of pathological ROS, we evaluated the role of NADPH oxidase (NOX) by inhibiting its activity using the non-specific NOX inhibitor, DPI.

Our data demonstrate that inhibition of NOX resulted in no change in beating rate when supplemented with normal (p=0.067) or high (p=0.061) glucose compared to baseline conditions (**Figure 6B**). Importantly however, there was a reduction in the number of EBs exhibiting beating activity when DPI was administered i.e., where 3 out of 10 EBs ceased activity when supplemented in normal glucose and 7 out of 17 in high glucose. (**Appendix B3**).

Morphologically, EB diameter showed no statistical change when cultured in high glucose compared to baseline (p=0.1488). Similarly, NOX inhibition in high glucose showed no change in EB diameter compared to baseline (p=0.451) or its' vehicle control (p>0.999) (**Figure 6A**). To test if NOX inhibition increased oxidative stress in hyperglycaemic-induced cardiac remodelling, we performed western blots, probing for nitrotyrosine. Western blot analysis showed no detectable levels of nitrotyrosine (**Appendix B3**).

To further study the effects of NOX in hyperglycaemia-induced cardiac remodelling, we examined cell viability and proliferation in NOX-inhibited EBs. Qualitatively, we found that DPI treatment had little EdU-positive nuclei (n=3) (**Appendix B3**).

Quantitatively, the percent PI-positive cells in DPI-treated groups were comparable to both baseline conditions (p > 0.99) and the high glucose-treated group (p=0.8319), showing no statistical significance (**Appendix B5**). High glucose treatment showed no change in PI-positive cells compared to baseline (p=0.1063). However, there was a significant increase in pyknotic-like nuclei when EBs were subjected to high glucose compared to the baseline control (p=0.0116). Furthermore, a substantial decrease in pyknotic-like nuclei was observed

when treated with DPI in a high glucose environment compared to its vehicle control (p=0.0009). Further, there was no alteration in pyknotic-like nuclei compared to baseline glucose (p=0.2733) (**Appendix B5**).

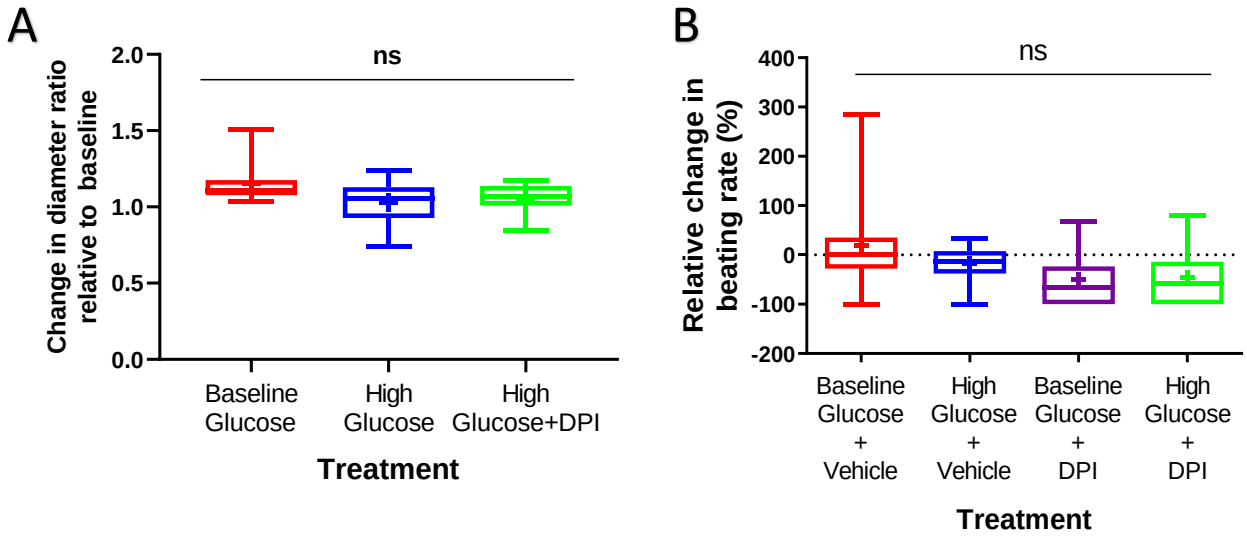

Figure 6: Pharmacological inhibition of NOX in beating stem cell-derived cardiac-like cells. *A) Relative change in diameter. n=3 independent culture batches with n=9-14 EBs per group B) Relative change in beating rate (n=10-16 EBs per group). Data represented as box and whisker plot, with the mean depicted as "+".*

4.3 Effect of hyperglycaemia-induced stress on p38 MAPK activity

To assess the involvement of p38 MAPK in hyperglycaemia-induced cardiac remodelling, we examined the expression levels of phospho-p38 MAPK and total p38 MAPK in EB cell homogenates by western blot. Qualitatively, western blots showed (**Figure 7A**) increased pp38 MAPK expression in high glucose conditions compared to normal glucose. Moreover, hydrogen peroxide treatment also increased pp38 MAPK expression. Total p38 MAPK expression remained constant across all groups (**Figure 7B**). Semi-quantification of active p38 MAPK (pp38 MAPK), relative to total p38 MAPK, revealed a significantly higher expression in high glucose conditions ($p=0.0016$) and hydrogen peroxide ($p=0.0010$) compared to baseline control conditions (**Figure 7C**).

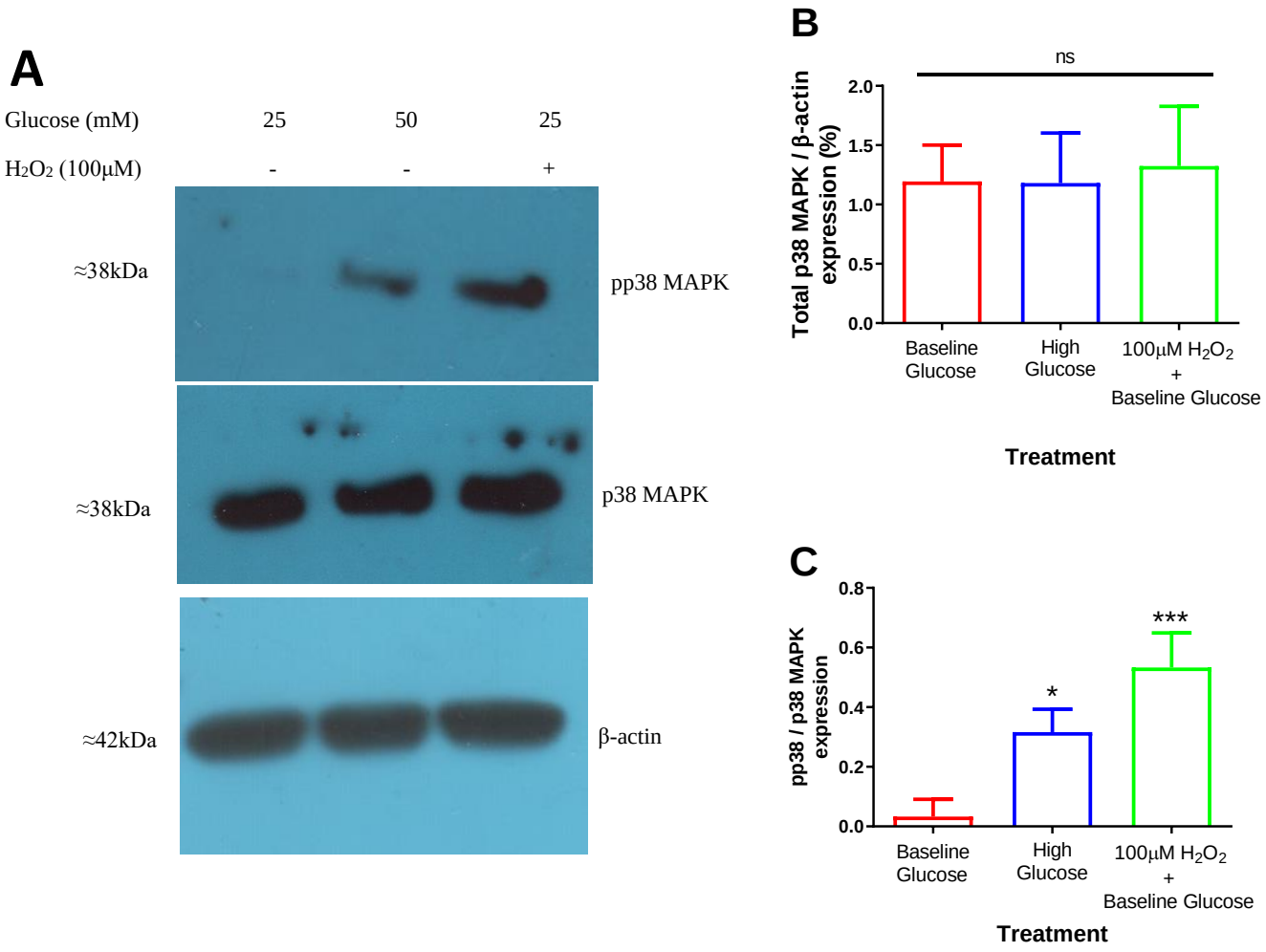

Figure 7: High glucose stimulates p38 MAPK activity in cardiac-like cells. ***A)*** *Representative western blot showing treatment with baseline glucose, high glucose, and hydrogen peroxide (100µM) probed for expression levels of pp38 MAPK, total p38 MAPK, and β-actin - serving as the protein loading control.* ***B)*** *Densitometric analysis of total p38 MAPK relative to β-actin protein expression.* ***C)*** *p38 MAPK activity (pp38 MAPK/p38 MAPK). Data presented as means ± SD (N=3) with significant (*P≤0.05, **P≤0.01, ***P≤0.001) compared to baseline glucose.*

4.4 Effect of p38 MAPK inhibition on cardiac-like EBs

The increase in p38 MAPK activity led us to investigate the role of p38 MAPK in high glucose conditions. Cell proliferation and viability were evaluated in pulsatile cardiac-like EBs, by inhibiting their activity with SB203580.

Qualitatively, EdU uptake looked slightly lower in high glucose-treated samples compared to baseline conditions (**Figure 8A**). SB20350 treatment seemed to partially attenuate the reduced EdU uptake from high glucose (**Figure 8A**). Quantitative analysis revealed significantly higher levels of EdU-positive nuclei in baseline glucose compared to high glucose, which was approximately 23.26% lower ($p=0.0190$). Inhibition of p38MAPK resulted in an increase of EdU uptake of 18.3% compared to high glucose alone, however, this change was of no statistical significance ($p=0.104$) (**Figure 8B**). Additionally, inhibition of p38 MAPK showed no statistical difference compared to baseline control ($p=0.7274$) (**Figure 8B**).

Further, the cell viability assay showed no statistical change, in PI uptake, across all groups, with high glucose exhibiting no alterations in PI levels compared to baseline ($p=0.1136$) and p38 MAPK inhibition not being different from baseline ($p=0.8270$) or high glucose alone ($p>0.999$) (**Appendix B5**). Data also indicate that inhibition of p38 MAPK partially mitigated the increase in pyknotic-like nuclei phenomena in high glucose treatment, with statistical significance not reached ($p=0.2544$) (**Figure 8C**). Moreover, levels of pyknotic-like nuclei in the p38 MAPK-inhibited group showed no statistical difference versus the baseline control ($p=0.6727$) (**Figure 8C**).

Qualitatively, GATA4 expression remained undetected across all groups (**Appendix B6**).

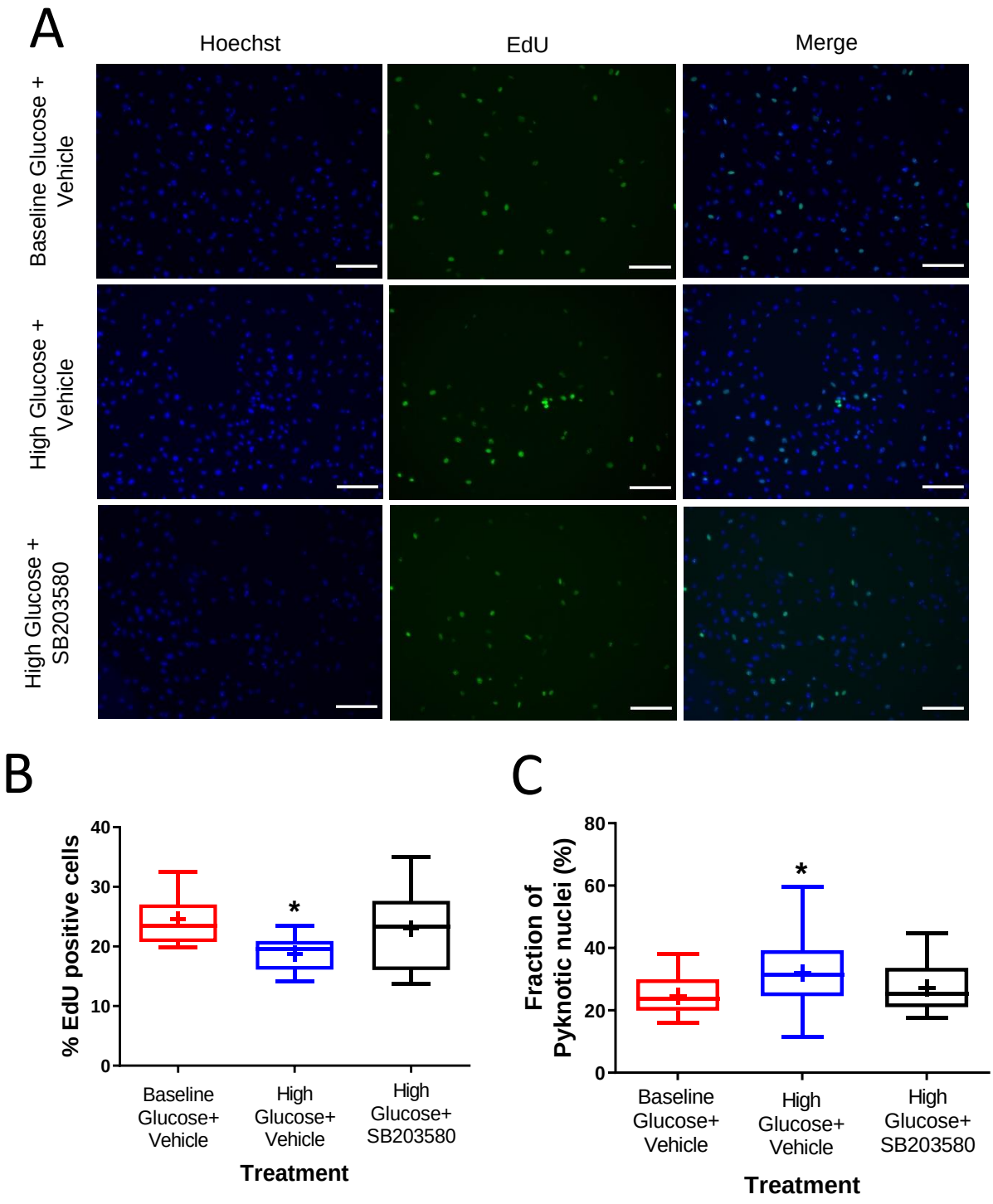

Figure 8: Pharmacological inhibition of p38 MAPK in stem-cell derived cardiac-like cells. ***A)*** *Representative fluorescence microscopy images of Hoechst (Blue), EdU (green), and merged images. Scale bar = 150μM.* ***B)*** *Quantitative analysis of the %EdU positive nuclei relative to total (n=3 independent cell culture batches, with n=4 EBs per group.* **C)** *Pyknotic-like nuclei relative to total nuclei (n=3 independent cell culture batches, with n=4-8 EBs per group). Data represented as a box and whisker plot, with the mean shown as "+" with significance (*P≤0.05) compared to baseline glucose.*

4.5 p38 MAPK signalling in mitochondrial homeostasis

Previous studies have shown mitochondria susceptibility to ROS under pathological conditions, with data indicating that mitochondrial fission and fusion are regulated via a p38 MAPK-dependent pathway (40,96). We investigated the role of p38 MAPK on mitochondrial homeostasis by examining the expression levels of the mitochondrial fusion protein optic atrophy-1 (OPA1) by western blot. Qualitatively, there was a reduction in OPA1 protein expression in high glucose compared to the baseline control. Furthermore, inhibition of p38 MAPK attenuated this decrease, where OPA1 expression was comparable to the baseline control (**Figure 9A**). Densitometric results showed a significant reduction in OPA1 expression (normalised to β-actin) in high glucose relative to baseline conditions ($p=0.0010$). Inhibition of p38 MAPK exhibited expression like baseline conditions ($p=0.2895$). Additionally, SB203580 treatment mitigated the effects observed in high glucose exhibiting a significant increase in OPA1 expression ($p=0.0041$) (**Figure 9B**).

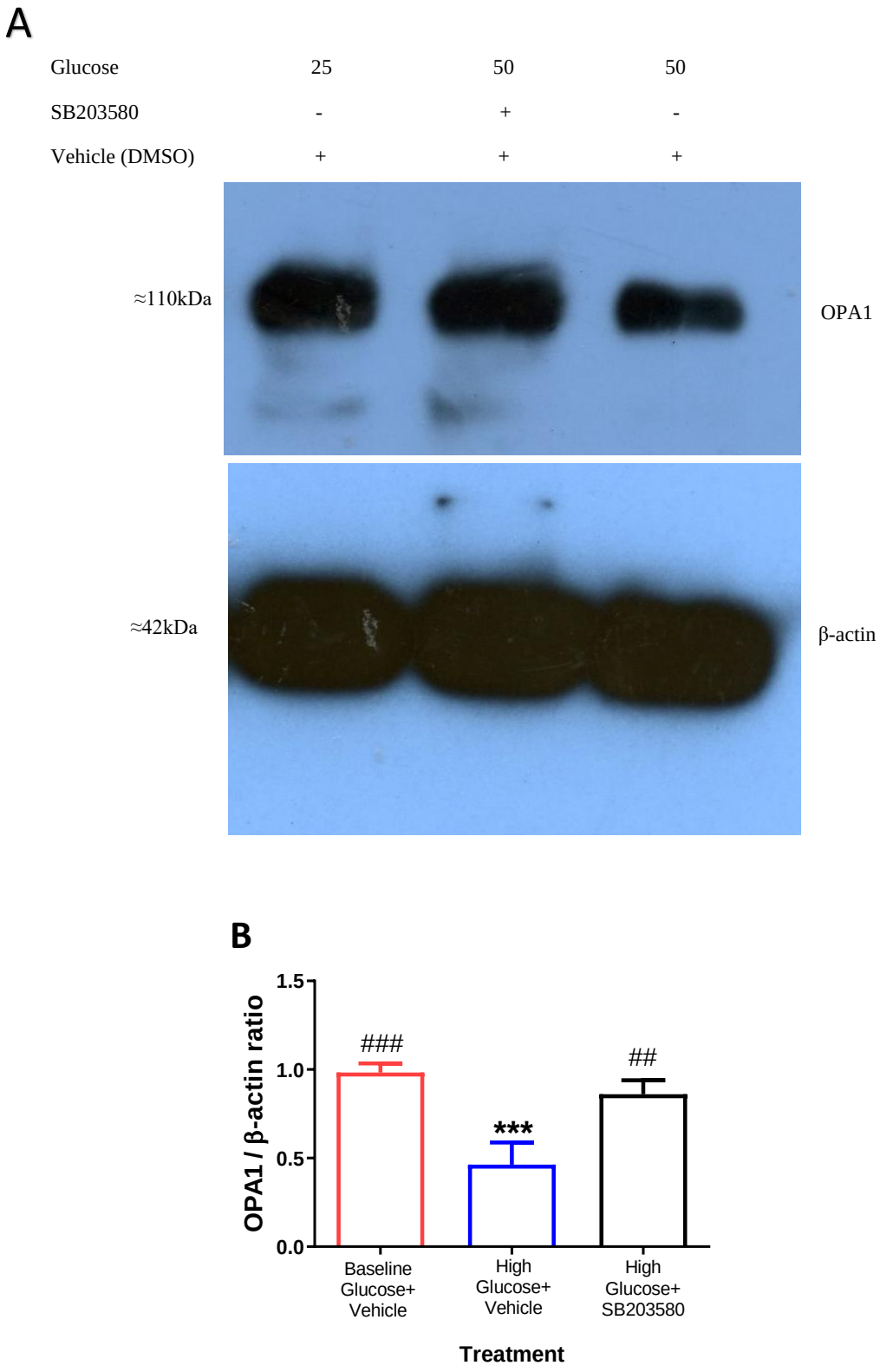

Figure 9: OPA1 expression in stem cell-derived cardiac-like cells. ***A)*** *Representative western blot treated with baseline (25mM) or high (50mM) glucose, supplemented with SB203580 (5μM) or vehicle (DMSO) and probed with OPA1 and β-actin – serving as the loading control.* ***B)*** *Densitometric analysis of OPA1 relative to B-actin protein expression. Data presented as mean± SD (N=3) with significant (*P≤0.05, **P≤0.01, ***P≤0.001) compared to baseline glucose or ($^{\#}$P≤0.05, $^{\#\#}$P≤0.01, $^{\#\#\#}$P≤0.001) compared to high glucose.*

5. Discussion

In this study, we successfully differentiated mouse embryonic stem cells into pulsatile cardiac-like cells via cell aggregate formation as demonstrated in other studies (97–99). In the same cellular model, these pulsatile mESC-derived cardiac-like EBs have been shown to express contractile proteins in addition to cardiac markers like cardiac troponin and α-actinin 2 proteins (84), indicating their cardiac-like nature. The current data also support these previous findings by showing a positive expression for F-actin in EBs. In this study, the expression of GATA4 (a marker of active cardiac differentiation) was not detected in pulsatile EBs, suggesting that pulsatile EBs have undergone cell commitment and successfully differentiated and matured into cardiac-like EBs. GATA4 is one of the early cardiac genes expressed during cardiac differentiation (100) and regulates the genes essential for early cardiomyogenesis (100,101). In contrast, other researchers have shown an increase in GATA4 expression from day 4-6 of their differentiation protocol until beating onset at day 8-12 (101). The differences between the result in the present study and other studies could be due to the unique properties of the cell lines used. Another possible explanation for the absence of GATA4 could be a time-dependent factor, as the pulsatile EBs tested in our study were between days 17 and 22. Given that GATA4 can self-regulate its expression, it may be suppressing its expression.

Using our cardiac-stem cell model, we showed that acute exposure to a known pro-oxidant hydrogen peroxide (100μM) produced a mild model of oxidative stress as evidenced by the lack of nitrotyrosine detection. The absence of nitrotyrosine may suggest that either there was insufficient ROS or the acute exposure of EBs (102) to the respective treatments was insufficient to produce long-term nitration of proteins. A similar pattern produced by high

glucose indicate that both treatments elicited a mild level of oxidative stress. Furthermore, the concentration of hydrogen peroxide (100μM) was sufficient to produce oxidative stress without it not being lethal to our cardiac-like EBs. Treatment with excessive concentrations of hydrogen peroxide (1mM) resulted in a complete loss of all functional activity, a loss of cell adhesion, and major EB breakdown and disintegration within a 24-hour time frame. These results correlate with findings performed by Ransy et al. (2020) who analysed the average dose of hydrogen peroxide required to produce oxidative damage in cellular models (103) and reported that 84% of publications (on a PubMed database search) use concentrations of hydrogen peroxide above 100μM (103).

In this study, hyperglycaemia exhibited no significant change in EB diameter, cell viability, or beating activity. However, an inspection of nuclei integrity and fragmentation for signs of pyknosis revealed that hyperglycaemic conditions showed significantly elevated levels of pyknotic-like nuclei compared to normoglycaemia conditions, which may suggest that hyperglycaemia may detrimentally affect these cells. Moreover, we demonstrated that treatment with hydrogen peroxide resulted in a significant decrease in EB diameter and cell viability. These alterations were likely triggered by increased ROS. While no significant changes were observed from hyperglycaemic treatment compared to baseline conditions, it is important to note that data indicated that there was also an insignificant change in both EB diameter and PI-positive nuclei in the hyperglycaemic group compared to our oxidative stress control. While the effects occurring in our hyperglycaemic group may not have closely mimicked our oxidative stress control, it did seem to have an intermediatory effect between baseline and the hydrogen peroxide treatment. As such, these differences may be attributed to the fact that hydrogen peroxide is directly stimulating our EBs with ROS, whereas hyperglycaemia treatment, is producing less ROS, at a more controlled concentration, and

hence the degree of oxidative stress from hyperglycaemia may be milder than that of hydrogen peroxide. Together, these suggest that in our cell line, 50mM glucose is sufficient to cause a mild form of oxidative stress. These data correlate with the results from other groups in both *in vivo* and *vitro* models, for example, Cao et al. demonstrated that high glucose-induced cardiomyocyte injury had significantly elevated levels of ROS coupled with reduced cell survival (104,105).

Given the alterations in EB size and viability when challenged with hydrogen peroxide, NADPH oxidase – a known source of ROS was investigated. Inhibition of NADPH oxidase (NOX) with DPI indicated that its suppression reduced the beating rates of cardiac-like EBs, irrespective of glucose concentration – with approximately 39% of EBs completely losing functional activity. This finding supports data from other groups showing reduced beating activity in cardiac-like EBs treated with DPI (45). Notably, the inhibition of NOX decreased cell proliferation without altering cell viability, suggesting that physiological levels of NOX-sourced ROS are vital for beating activity and cell proliferation. These findings, however, may be due to off-target effects. Typically, DPI is used for the non-specific inhibition of NOX however, several reports suggest that not only does DPI affect NOX, but also other flavoenzymes like xanthine oxidase and nitric oxide synthase (106). Other effects of DPI include inhibition of mitochondrial ROS (107); promotion of apoptosis via superoxide (O_2^-) mediated process; impeding ROS metabolism (108), and non-selectively inhibiting ion channels (109). Given these broad effects, it might be the cause of contradicting effects when comparing findings (110). Therefore, the role and contribution of ROS from NOX remain unclear. However, consistent with a study by Kučera et al., NOX inhibition with DPI resulted in reduced cell proliferation. They attributed this to DPI having a pro-oxidant effect via the

impairment of the pentose phosphate pathway (PPP) where the inhibition of PPP reduced NADPH synthesis – a crucial cofactor implicated in several antioxidant systems (108,110).

DPI has also been reported to regulate ion channel activity (109). Inhibition and blockage of voltage-gated and calcium-dependent (K_v and K_{Ca}^{2+}) channels by DPI reduced the proliferation of cancer cells in breast and prostate (111), glial cells (111), bone marrow-derived mesenchymal stem cells (MSCs) from mice (112), and rat cardiac fibroblasts (113). Blockage of such channels by DPI may account for reduced beating activity and cell proliferation, however, this requires further testing. Altogether, these data indicate that high glucose (50mM) induces a mild form of oxidative stress, having an insignificant effect on EB size and cell viability while inducing a pyknotic-like phenomenon. Furthermore, we found that the alterations from hyperglycaemia are unlikely to be acting via NOX, however, evidence remains inconclusive because although pharmacological inhibition of NOX with DPI may be blocking its activity, we cannot rule out the possibility that our observations were from the modulation of alternative biological targets.

In the present study, hyperglycaemia promoted p38 MAPK activity without affecting total p38 MAPK. This is likely to be via ROS-dependent signalling, with hydrogen peroxide having the same effect on p38 MAPK activity. Other groups have also reported elevated p38 MAPK activity in cardiomyocytes in hyperglycaemic conditions (73). A study by Li et al. demonstrated that physiological ROS is vital for early cardiac differentiation, acting via the p38 MAPK pathway – with inhibition of p38 MAPK abrogating cell differentiation (45). Although several studies indicate that p38 MAPK activity is detrimental in mature cardiomyocytes, some suggest the outcome is isoform dependent, with p38β MAPK modulating a protective role against pathology with the more dominant α isoform is harmful.

A further investigation into the role of p38 MAPK on our cardiac-like EBs during hyperglycaemia revealed that it may be implicated in reducing cell proliferation and survival. The non-specific inhibition of p38 MAPK with SB203580 may be partially attenuating the effects of hyperglycaemia on both cell survival and cell proliferation without promoting cardiac maturation as evidenced by the absence of GATA4 expression. Evidence presented by other groups has demonstrated that p38 MAPK inhibition attenuated the effects of hyperglycaemia on both cell proliferation and cell survival (68,114–116). While the extent of the changes observed by other groups does not fully correlate with our study, it is important to note that our sample size was small ($n \geq 4$) and hence increasing the type 2 (beta) error rate. As such, it was difficult to identify trends that may occur, and a definitive conclusion cannot be made.

Our data also showed hyperglycaemia significantly reduced the expression of the mitochondrial fusion protein, OPA1, with p38 MAPK inhibition attenuating this effect. Mitochondrial fission and fusion are critical processes required for maintaining mitochondria when cells are under environmental and metabolic stresses (96). Fusion is a process mediated by OPA1 and helps alleviate stress by combining and thus complementing the contents of partially damaged mitochondria. Fission is the process where new mitochondria are created, with it also being vital for the removal of damaged mitochondria – thus facilitating apoptosis during cellular stress and is mediated by dynamin-related protein-1 (DRP1) (96). Previous reports indicated that hyperglycaemia stimulates DRP1 expression, thus promoting mitochondrial fission (117). Further, DRP1-mediated mitochondrial fission was susceptible to SB203580, where inhibition of p38 MAPK – located upstream of DRP1 – reduced DRP phosphorylation and thus its activation (118).

Mitochondrial fission and fusion are dynamic and competing processes i.e., compensate for damage by fusing and removing damaged organelles by fission (96). Therefore,

hyperglycaemia may promote cell death by fission and hence reduces fusion, evident by the decrease in fusion machinery. Higher levels of OPA1 were observed when treated with SB203580. This change may be a compensatory mechanism, where mitochondria are hyper-fused to increased metabolic stress and may be acting via a p38 MAPK-dependent pathway. Conversely, inhibition of p38 MAPK might disrupt physiological processes by preventing the segregation of compromised mitochondria from healthy ones. Therefore, damaged mitochondria are fused with healthy ones – resulting in mitochondrial dysfunction. It could further explain our data demonstrating the inhibition of p38 MAPK only partially mitigated the effects of hyperglycaemia in causing a pyknotic-like phenomenon and reducing proliferation. However, this remains elusive and requires further investigation.

Together, these data suggest that hyperglycaemia reduces cell proliferation, detrimentally affects cell health, compromised mitochondrial regulation, and is likely acting via a p38 MAPK-dependent signalling pathway. Given the improvement in the effects of hyperglycaemia, pharmacological inhibition of p38 MAPK in addition to conventional anti-diabetic therapy could serve as a therapeutic target for treating diabetic cardiomyopathy.

This study provided insight into changes that occur from a hyperglycaemic environment and the possible involvement of p38 MAPK. However, to understand the exact mechanism behind the pathology, further areas need to be dissected. Given that p38 MAPK consists of several isoforms and the inhibitor used blocks p38 MAPK irrespective of its isoform, the function, and expression of each isoform need to be investigated - especially the lesser characterised p38 MAPK isoforms i.e., p38δ and p38γ.

A large portion of this study investigated the overall outcome caused by p38 MAPK activation by hyperglycaemia stimulation. However, the transcription factors downstream of

p38 MAPK leading to these alterations were not explored. Given the identified importance of p38 MAPK in regulating cell proliferation, downstream proteins, and genes sensitive to p38 MAPK and implicated in the cell cycle should be further explored. These include p53 (119), TGF-β (120), and p21Cip (121), however, most of these were identified in cancer cell lines and therefore require further characterization within cardiac-specific models.

6. Conclusion

This study demonstrated that, in a developmental model of the heart, hyperglycaemia induced a pyknotic-like phenomenon, suppressed cell proliferation, and reduced the expression of mitochondrial fusion proteins in mESC-derived cardiac-like cells. These effects were likely triggered by oxidative stress and acted via the p38 MAPK signalling pathway as summarized in Figure 10. These results suggest hyperglycaemia may induce a pathological change via the p38 MAPK signalling cascade in developing cardiac cells. These findings provide insight into hyperglycaemic-induced cardiac remodelling and may clinically implicate this signalling pathway in diabetes-induced cardiomyocyte remodelling.

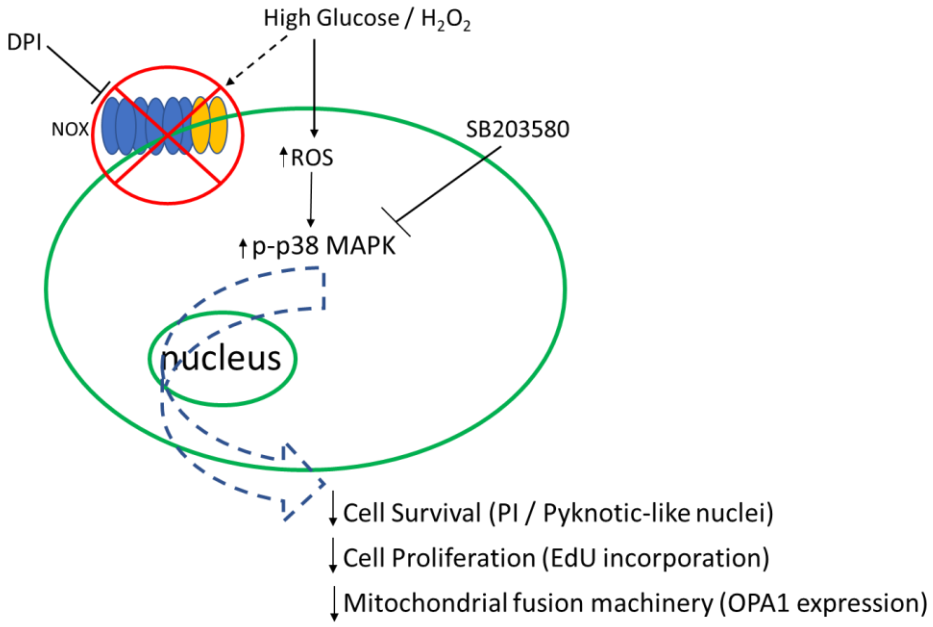

Figure 10. Model depicting signalling pathway involved in hyperglycaemia-induced cardiac remodelling in a stem cell model. *High glucose induced oxidative stress stimulates p38 MAPK activity, resulting in reduced cell proliferation, survival, and a downregulation of the mitochondria fusion protein, OPA1.*

7. References

1. Saeedi P, Petersohn I, Salpea P, Malanda B, Karuranga S, Unwin N, et al. Global and regional diabetes prevalence estimates for 2019 and projections for 2030 and 2045: Results from the International Diabetes Federation Diabetes Atlas, 9(th) edition. Diabetes Res Clin Pract. 2019 Nov;157:107843.

2. Williams R, Colagiuri S, Chan J, Gregg E, Ke C, Lim L-L, et al. IDF Atlas 9th Edition 2019. 2019.

3. Kahanovitz L, Sluss PM, Russell SJ. Type 1 diabetes-a clinical perspective. Point Care. 2017;16(1):37–40.

4. Barquilla García A. Brief update on diabetes for general practitioners. Rev Esp Sanid Penit. 2017;19(2):57–65.

5. Roever L, Casella-Filho A, Dourado PM, Resende E, Chagas A. Cardiovascular-complications-in-diabetes. 2014 Dec 6;

6. Azevedo PS, Polegato BF, Minicucci MF, Paiva SAR, Zornoff LAM. Cardiac Remodeling: Concepts, Clinical Impact, Pathophysiological Mechanisms and Pharmacologic Treatment. Arq Bras Cardiol. 2016;106(1):62–9.

7. Marwick TH. Measurement of strain and strain rate by echocardiography: Ready for prime time? J Am Coll Cardiol. 2006;47(7):1313–27.

8. Kaushik A, Kapoor A. Use of strain, strain rate, tissue velocity imaging and endothelial function for early detection of cardiovascular involvement in young diabetics. Indian Heart J [Internet]. 2018;70:S45. Available from: https://doi.org/10.1016/j.ihj.2018.11.006

9. Yoneyama K, Venkatesh BA, Wu CO, Mewton N, Gjesdal O, Kishi S, et al. Diabetes mellitus and insulin resistance associate with left ventricular shape and torsion by cardiovascular magnetic resonance imaging in asymptomatic individuals from the multi-ethnic study of atherosclerosis. J Cardiovasc Magn Reson. 2018;20(1):53.

10. Klein BEK, Klein R, Lee KE. Components of the metabolic syndrome and risk of cardiovascular disease and diabetes in Beaver Dam. Diabetes Care. 2002 Oct;25(10):1790–4.

11. Taegtmeyer H, Golfman L, Sharma S, Razeghi P, van Arsdall M. Linking gene expression to function: metabolic flexibility in the normal and diseased heart. Ann N Y Acad Sci. 2004 May;1015:202–13.

12. Nather K. Investigating angiotensin ii in cardiac remodelling and the counter-regulatory actions of angiotensin-(1-9). PQDT - UK Irel [Internet]. 2016; Available from: https://manchester.idm.oclc.org/login?url=https://search.proquest.com/docview/1896110611?accountid=12253%0Ahttp://man-fe.hosted.exlibrisgroup.com/openurl/44MAN/44MAN_services_page?genre=dissertations+%26+theses&atitle=&author=Nather%2C+Katrin&volume=&issu

13. Cox EJ, Marsh SA. A systematic review of fetal genes as biomarkers of cardiac hypertrophy in rodent models of diabetes. PLoS One. 2014;9(3):1–11.

14. Batalov I, Feinberg AW. Bmi-Suppl.1-2015-071-1. 2015;10:71–6.

15. Aykac I, Podesser BK, Kiss A. Reverse remodeling in diabetic cardiomyopathy: the role of extracellular matrix. Minerva Cardiol Angiol [Internet]. 2022;70(3):385–92. Available from: http://europepmc.org/abstract/MED/34713679

16. Swynghedauw B. Molecular mechanisms of myocardial remodeling. Physiol Rev. 1999 Jan;79(1):215–62.

17. Dhalla NS, Shah AK, Tappia PS. Role of oxidative stress in metabolic and subcellular abnormalities in diabetic cardiomyopathy. Int J Mol Sci. 2020;21(7).

18. Pierce GN, Russell JC. Regulation of intracellular Ca2+ in the heart during diabetes. Cardiovasc Res [Internet]. 1997 Apr 1;34(1):41–7. Available from: https://doi.org/10.1016/S0008-6363(97)00010-2

19. Schirone L, Forte M, Palmerio S, Yee D, Nocella C, Angelini F, et al. A Review of the Molecular Mechanisms Underlying the Development and Progression of Cardiac Remodeling. Oxid Med Cell Longev [Internet]. 2017/07/02. 2017;2017:3920195. Available from: https://pubmed.ncbi.nlm.nih.gov/28751931

20. Koshman YE, Sternlicht MD, Kim T, O'Hara CP, Koczor CA, Lewis W, et al. Connective tissue growth factor regulates cardiac function and tissue remodeling in a mouse model of dilated cardiomyopathy. J Mol Cell Cardiol. 2015 Dec;89(Pt B):214–22.

21. Mandavia CH, Aroor AR, Demarco VG, Sowers JR. Molecular and metabolic mechanisms of cardiac dysfunction in diabetes. Life Sci. 2013 Mar;92(11):601–8.

22. Rawal S, Nagesh PT, Coffey S, Van Hout I, Galvin IF, Bunton RW, et al. Early dysregulation of cardiac-specific microRNA-208a is linked to maladaptive cardiac remodelling in diabetic myocardium. Cardiovasc Diabetol [Internet]. 2019;18(1):1–12. Available from: https://doi.org/10.1186/s12933-019-0814-4

23. Jia G, Whaley-Connell A, Sowers JR. Diabetic cardiomyopathy: a hyperglycaemia- and insulin-resistance-induced heart disease. Diabetologia. 2018 Jan;61(1):21–8.

24. Jha JC, Ho F, Dan C, Jandeleit-Dahm K. A causal link between oxidative stress and inflammation in cardiovascular and renal complications of diabetes. Clin Sci [Internet]. 2018 Aug 30;132(16):1811–36. Available from: https://doi.org/10.1042/CS20171459

25. Yang P, Feng J, Peng Q, Liu X, Fan Z, Luca M. Advanced Glycation End Products: Potential Mechanism and Therapeutic Target in Cardiovascular Complications under Diabetes. Oxid Med Cell Longev. 2019;2019.

26. Pedicino D, Liuzzo G, Trotta F, Giglio AF, Giubilato S, Martini F, et al. Adaptive Immunity, Inflammation, and Cardiovascular Complications in Type 1 and Type 2 Diabetes Mellitus. Cameron N, editor. J Diabetes Res [Internet]. 2013;2013:184258. Available from: https://doi.org/10.1155/2013/184258

27. Shah MS, Brownlee M. Molecular and cellular mechanisms of cardiovascular disorders in diabetes. Circ Res. 2016;118(11):1808–29.

28. Rodríguez-Rodríguez P, Ramiro-Cortijo D, Reyes-Hernández CG, López de Pablo AL, Carmen González M, Arribas SM. Implication of oxidative stress in fetal programming of cardiovascular disease. Front Physiol. 2018;9(MAY):1–13.

29. Shen X, Zheng S, Metreveli NS, Epstein PN. Protection of cardiac mitochondria by overexpression of MnSOD reduces diabetic cardiomyopathy. Diabetes. 2006 Mar;55(3):798–805.

30. Wilson AJ, Gill EK, Abudalo RA, Edgar KS, Watson CJ, Grieve DJ. Reactive oxygen species signalling in the diabetic heart : emerging prospect for therapeutic targeting. 2018;293–9.

31. Hansen SS, Aasum E, Hafstad AD. The role of NADPH oxidases in diabetic cardiomyopathy. Biochim Biophys Acta - Mol Basis Dis [Internet]. 2018;1864(5):1908–13. Available from: http://dx.doi.org/10.1016/j.bbadis.2017.07.025

32. Duncan JG. Mitochondrial dysfunction in diabetic cardiomyopathy. Biochim Biophys Acta. 2011 Jul;1813(7):1351–9.

33. Shen X, Zheng S, Thongboonkerd V, Xu M, Pierce WM, Klein JB, et al. Cardiac mitochondrial damage and biogenesis in a chronic model of type 1 diabetes. Am J Physiol - Endocrinol Metab. 2004;287(5 50-5):896–905.

34. Chung HS, Wang S-B, Venkatraman V, Murray CI, Van Eyk JE. Cysteine oxidative posttranslational modifications: emerging regulation in the cardiovascular system. Circ Res. 2013 Jan;112(2):382–92.

35. Hu X-F, Wang L, Xiang G, Lei W, Feng Y-F. Angiogenesis impairment by the NADPH oxidase-triggered oxidative stress at the bone-implant interface: Critical mechanisms and therapeutic targets for implant failure under hyperglycemic conditions in diabetes. Acta Biomater. 2018 Jun;73:470–87.

36. Breitkreuz M, Hamdani N. A change of heart: oxidative stress in governing muscle function? Biophys Rev. 2015;7(3):321–41.

37. Wang Z, Hall SD, Maya JF, Li L, Asghar A, Gorski JC. Diabetes mellitus increases the in vivo activity of cytochrome P450 2E1 in humans. Br J Clin Pharmacol. 2003;55(1):77–85.

38. Veith A, Moorthy B. ROLE OF CYTOCHROME P450S IN THE GENERATION AND METABOLISM OF REACTIVE OXYGEN SPECIES. Curr Opin Toxicol [Internet]. 2017/10/12. 2018 Feb;7:44–51. Available from: https://pubmed.ncbi.nlm.nih.gov/29527583

39. Kayama Y, Raaz U, Jagger A, Adam M, Schellinger IN, Sakamoto M, et al. Diabetic cardiovascular disease induced by oxidative stress. Int J Mol Sci. 2015;16(10):25234–63.

40. Nishikawa T, Edelstein D, Du XL, Yamagishi S, Matsumura T, Kaneda Y, et al. Normalizing mitochondrial superoxide production blocks three pathways of hyperglycaemic damage. Nature. 2000 Apr;404(6779):787–90.

41. Guo CY, Sun L, Chen XP, Zhang DS. Oxidative stress, mitochondrial damage and neurodegenerative diseases. Neural Regen Res. 2013;8(21):2003–14.

42. Ekelund UE, Harrison RW, Shokek O, Thakkar RN, Tunin RS, Senzaki H, et al. Intravenous allopurinol decreases myocardial oxygen consumption and increases mechanical efficiency in dogs with pacing-induced heart failure. Circ Res. 1999 Sep;85(5):437–45.

43. Amado LC, Saliaris AP, Raju SVY, Lehrke S, St. John M, Xie J, et al. Xanthine oxidase inhibition ameliorates cardiovascular dysfunction in dogs with pacing-induced heart failure. J Mol Cell Cardiol. 2005;39(3):531–6.

44. Rastogi R, Geng X, Li F, Ding Y. NOX activation by subunit interaction and underlying mechanisms in disease. Front Cell Neurosci. 2017;10(January):1–13.

45. Li J, Stouffs M, Serrander L, Banfi B, Bettiol E, Charnay Y, et al. The NADPH oxidase NOX4 drives cardiac differentiation: Role in regulating cardiac transcription factors and MAP kinase activation. Mol Biol Cell [Internet]. 2006/06/14. 2006 Sep;17(9):3978–88. Available from: https://pubmed.ncbi.nlm.nih.gov/16775014

46. Maalouf RM, Eid AA, Gorin YC, Block K, Escobar GP, Bailey S, et al. Nox4-derived reactive oxygen species mediate cardiomyocyte injury in early type 1 diabetes. Am J Physiol Cell Physiol. 2012 Feb;302(3):C597-604.

47. Shen E, Li Y, Li Y, Shan L, Zhu H, Feng Q, et al. Rac1 is required for cardiomyocyte apoptosis during hyperglycemia. Diabetes. 2009 Oct;58(10):2386–95.

48. Li Y, Li Y, Feng Q, Arnold M, Peng T. Calpain activation contributes to hyperglycaemia-induced apoptosis in cardiomyocytes. Cardiovasc Res [Internet]. 2009 Jun 8;84(1):100–10. Available from: https://doi.org/10.1093/cvr/cvp189

49. Joseph D, Kimar C, Symington B, Milne R, Essop MF. The detrimental effects of acute hyperglycemia on myocardial glucose uptake. Life Sci [Internet]. 2014;105(1–2):31–42. Available from: http://europepmc.org/abstract/MED/24747137

50. Watanabe K, Thandavarayan RA, Harima M, Sari FR, Gurusamy N, Veeraveedu PT, et al. Role of differential signaling pathways and oxidative stress in diabetic cardiomyopathy. Curr Cardiol Rev. 2010 Nov;6(4):280–90.

51. Hayashi T, Mori T, Yamashita C, Miyamura M. Regulation of Oxidative Stress and Cardioprotection in Diabetes Mellitus. Curr Cardiol Rev. 2008;4(4):251–8.

52. McMullen JR, Shioi T, Zhang L, Tarnavski O, Sherwood MC, Kang PM, et al. Phosphoinositide 3-kinase(p110alpha) plays a critical role for the induction of physiological, but not pathological, cardiac hypertrophy. Proc Natl Acad Sci U S A. 2003 Oct;100(21):12355–60.

53. Son Y, Cheong Y-K, Kim N-H, Chung H-T, Kang DG, Pae H-O. Mitogen-Activated Protein Kinases and Reactive Oxygen Species: How Can ROS Activate MAPK Pathways? J Signal Transduct. 2011;2011:1–6.

54. Kostenko S. Physiological roles of mitogen-activated-protein-kinase-activated p38-regulated/activated protein kinase. World J Biol Chem. 2011;2(5):73.

55. Kyriakis JM, Avruch J. Mammalian mitogen-activated protein kinase signal transduction pathways activated by stress and inflammation. Physiol Rev. 2001 Apr;81(2):807–69.

56. Li Z, Jiang Y, Ulevitch RJ, Han J. The primary structure of p38γ: A new member of p38 group of MAP kinases. Biochem Biophys Res Commun. 1996;228(2):334–40.

57. Martin ED, Felice De Nicola G, Marber MS. New therapeutic targets in cardiology: P38 alpha mitogen-activated protein kinase for ischemic heart disease. Circulation. 2012;126(3):357–68.

58. Kumar S, Mcdonnell PC, Gum RJ, Hand AT, Lee JC, Young PR. Novel Homologues of CSBP / p38 MAP Kinase : Activation , Substrate Specificity and Sensitivity to Inhibition by Pyridinyl Imidazoles. 1997;538(235):533–8.

59. Allen M, Svensson L, Roach M, Hambor J, McNeish J, Gabel CA. Deficiency of the stress kinase p38α results in embryonic lethality: Characterization of the kinase dependence of stress responses of enzyme-deficient embryonic stem cells. J Exp Med. 2000;191(5):859–69.

60. Adams RH, Porras A, Alonso G, Jones M, Vintersten K, Panelli S, et al. Essential role of p38α MAP kinase in placental but not embryonic cardiovascular development. Mol Cell. 2000;6(1):109–16.

61. Sabio G, Arthur JSC, Kuma Y, Peggie M, Carr J, Murray-Tait V, et al. p38γ regulates the localisation of SAP97 in the cytoskeleton by modulating its interaction with GKAP. EMBO J. 2005;24(6):1134–45.

62. Lin Q, Lu J, Yanagisawa H, Webb R, Lyons GE, Richardson JA, et al. Requirement of the MADS-box transcription factor MEF2C for vascular development. Development [Internet]. 1998 Nov 15;125(22):4565 LP – 4574. Available from: http://dev.biologists.org/content/125/22/4565.abstract

63. Harvey RP. Seeking a regulatory roadmap for heart morphogenesis. Semin Cell Dev Biol. 1999 Feb;10(1):99–107.

64. Romero-Becerra R, Santamans AM, Folgueira C, Sabio G. P38 mapk pathway in the heart: New insights in health and disease. Int J Mol Sci. 2020;21(19):1–19.

65. Marks AR. Calcium cycling proteins and heart failure : mechanisms and therapeutics Find the latest version : Review series Calcium cycling proteins and heart failure : mechanisms and therapeutics. J Clin Invest [Internet]. 2013;123(1):46–52. Available from: http://www.jci.org/articles/view/62834

66. Arabacilar P, Marber M. The case for inhibiting p38 mitogen-activated protein kinase in heart failure. Front Pharmacol. 2015;6(MAY):1–7.

67. Kerkela R, Force T. p38 Mitogen-Activated Protein Kinase. A Future Target for Heart Failure Therapy?* * Editorials published in the Journal of the American College of Cardiology reflect the views of the authors and do not necessarily represent the views of JACC or the Americ. J Am Coll Cardiol. 2006;48(3):556–8.

68. Liao P, Wang SQ, Wang S, Zheng M, Zheng M, Zhang SJ, et al. P38 Mitogen-Activated Protein Kinase Mediates a Negative Inotropic Effect in Cardiac Myocytes. Circ Res. 2002;90(2):190–6.

69. Nemoto S, Sheng Z, Lin A. Opposing effects of Jun kinase and p38 mitogen-activated protein kinases on cardiomyocyte hypertrophy. Mol Cell Biol [Internet]. 1998 Jun;18(6):3518–26. Available from: https://pubmed.ncbi.nlm.nih.gov/9584192

70. Hoefer J, Azam MA, Kroetsch JTE, Poi HL, Momen MA, Voigtlaender-Bolz J, et al. Sphingosine-1-phosphate-dependent activation of p38 MAPK maintains elevated peripheral resistance in heart failure through increased myogenic vasoconstriction. Circ Res. 2010;107(7):923–33.

71. Widder J, Behr T, Fraccarollo D, Hu K, Galuppo P, Tas P, et al. Vascular endothelial dysfunction and superoxide anion production in heart failure are p38 MAP kinase-

dependent. Cardiovasc Res. 2004;63(1):161–7.

72. Kaiser RA, Bueno OF, Lips DJ, Doevendans PA, Jones F, Kimball TF, et al. Targeted Inhibition of p38 Mitogen-activated Protein Kinase Antagonizes Cardiac Injury and Cell Death Following Ischemia-Reperfusion in Vivo. J Biol Chem. 2004;279(15):15524–30.

73. Thandavarayan RA, Watanabe K, Ma M, Gurusamy N, Veeraveedu PT, Konishi T, et al. Dominant-negative p38α mitogen-activated protein kinase prevents cardiac apoptosis and remodeling after streptozotocin-induced diabetes mellitus. Am J Physiol - Hear Circ Physiol. 2009;297(3):911–9.

74. Koivisto E, Kaikkonen L, Tokola H, Pikkarainen S, Aro J, Pennanen H, et al. Distinct regulation of B-type natriuretic peptide transcription by p38 MAPK isoforms. Mol Cell Endocrinol [Internet]. 2011;338(1):18–27. Available from: http://www.sciencedirect.com/science/article/pii/S0303720711001523

75. Zhao Y, Tan Y, Xi S, Li Y, Li C, Cui J, et al. A novel mechanism by which SDF-1β protects cardiac cells from palmitate-induced endoplasmic reticulum stress and apoptosis via CXCR7 and AMPK/p38 MAPK-mediated interleukin-6 generation. Diabetes [Internet]. 2013/02/19. 2013 Jul;62(7):2545–58. Available from: https://pubmed.ncbi.nlm.nih.gov/23423573

76. Hescheler J, Fleischmann BK, Lentini S, Maltsev VA, Rohwedel J, Wobus AM, et al. Embryonic stem cells: A model to study structural and functional properties in cardiomyogenesis. Cardiovasc Res. 1997;36(2):149–62.

77. Sachinidis A, Fleischmann BK, Kolossov E, Wartenberg M, Sauer H, Hescheler J. Cardiac specific differentiation of mouse embryonic stem cells. Cardiovasc Res. 2003;58(2):278–91.

78. Cesarz Z, Tamama K. Spheroid Culture of Mesenchymal Stem Cells. Stem Cells Int. 2016;2016.

79. Llames S, García-Pérez E, Meana Á, Larcher F, Del Río M. Feeder Layer Cell Actions and Applications. Tissue Eng - Part B Rev. 2015;21(4):345–53.

80. Roy A, Krzykwa E, Lemieux R, Néron S. Increased efficiency of gamma-irradiated versus mitomycin C-treated feeder cells for the expansion of normal human cells in long-term cultures. J Hematother Stem Cell Res. 2001 Dec;10(6):873–80.

81. Wang X, Yang P. In vitro differentiation of mouse embryonic stem (mES) cells using the hanging drop method. J Vis Exp. 2008;(17):2–3.

82. Aboalgasm H, Ballo R, Mkatazo T, Gwanyanya A. Hyperglycaemia-Induced Contractile Dysfunction and Apoptosis in Cardiomyocyte-Like Pulsatile Cells Derived from Mouse Embryonic Stem Cells. Cardiovasc Toxicol [Internet]. 2021;21(9):695–709. Available from: https://doi.org/10.1007/s12012-021-09660-3

83. Polonchuk L, Chabria M, Badi L, Hoflack J-C, Figtree G, Davies MJ, et al. Cardiac spheroids as promising in vitro models to study the human heart microenvironment. Sci Rep [Internet]. 2017 Aug 1;7(1):7005. Available from: https://pubmed.ncbi.nlm.nih.gov/28765558

84. Aboalgasm H, Ballo R, Gwanyanya A. Organisational alteration of cardiac myofilament proteins by hyperglycaemia in mouse embryonic stem cell-derived

cardiomyocytes. J Muscle Res Cell Motil [Internet]. 2021;42(3–4):419–28. Available from: https://doi.org/10.1007/s10974-021-09607-9

85. Gorski DJ, Petz A, Reichert C, Twarock S, Grandoch M, Fischer JW. Cardiac fibroblast activation and hyaluronan synthesis in response to hyperglycemia and diet-induced insulin resistance. Sci Rep. 2019;9(1):1–11.

86. Viskupicova J, Blaskovic D, Galiniak S, Soszyński M, Bartosz G, Horakova L, et al. Effect of high glucose concentrations on human erythrocytes in vitro. Redox Biol. 2015;5:381–7.

87. Ali NN, Xu X, Brito-Martins M, Poole-Wilson PA, Harding SE, Fuller SJ. Beta-adrenoceptor subtype dependence of chronotropy in mouse embryonic stem cell-derived cardiomyocytes. Basic Res Cardiol [Internet]. 2004;99(6):382–91. Available from: https://doi.org/10.1007/s00395-004-0484-5

88. Guan K, Fürst DO, Wobus AM. Modulation of sarcomere organization during embryonic stem cell-derived cardiomyocyte differentiation. Eur J Cell Biol. 1999 Nov;78(11):813–23.

89. Crespo FL, Sobrado VR, Gomez L, Cervera AM, McCreath KJ. Mitochondrial reactive oxygen species mediate cardiomyocyte formation from embryonic stem cells in high glucose. Stem Cells. 2010;28(7):1132–42.

90. Han S, Wang G, Jin Y, Ma Z, Jia W, Wu X, et al. Investigating the Mechanism of Hyperglycemia-Induced Fetal Cardiac Hypertrophy. PLoS One. 2015;10(9):e0139141.

91. Xu X, Ruan L, Tian X, Pan F, Yang C, Liu G. Calcium inhibitor inhibits high glucose-induced hypertrophy of H9C2 cells. Mol Med Rep [Internet]. 2020;22(3):1783–92. Available from: https://doi.org/10.3892/mmr.2020.11275

92. Tirziu D, Chorianopoulos E, Moodie KL, Palac RT, Zhuang ZW, Tjwa M, et al. Myocardial hypertrophy in the absence of external stimuli is induced by angiogenesis in mice. J Clin Invest. 2007 Nov;117(11):3188–97.

93. Scientific T. Click-iT® EdU Imaging Kits. Imaging. 2011;2–5.

94. Haycock JW. Polyvinylpyrrolidone as a blocking agent in immunochemical studies. Anal Biochem. 1993 Feb;208(2):397–9.

95. Pierce Biotechnology. Western Blotting Handbook and Troubleshooting Guide Featuring the SuperSignal ® West Family of Products. 2004;

96. Youle RJ, Van Der Bliek AM. Good for Discussion: Mitochondrial Fission, Fusion, and Stress. Science (80-) [Internet]. 2012;337(6098):1062–5. Available from: https://www.ncbi.nlm.nih.gov/pmc/articles/PMC4762028/pdf/nihms757703.pdf

97. Pasquale E Di, Song B, Condorelli G. Generation of Human Cardiomyocytes: A Differentiation Protocol from Feeder-free Human Induced Pluripotent Stem Cells. J Vis Exp. 2013;(76):1–6.

98. Laflamme MA, Murry CE. Heart regeneration. Nature [Internet]. 2011;473(7347):326–35. Available from: https://doi.org/10.1038/nature10147

99. Mummery CL, Zhang J, Ng ES, Elliott DA, Elefanty AG, Kamp TJ. Differentiation of human embryonic stem cells and induced pluripotent stem cells to cardiomyocytes: a

methods overview. Circ Res. 2012 Jul;111(3):344–58.

100. Rossi JM, Dunn NR, Hogan BL, Zaret KS. Distinct mesodermal signals, including BMPs from the septum transversum mesenchyme, are required in combination for hepatogenesis from the endoderm. Genes Dev. 2001 Aug;15(15):1998–2009.

101. Yilbas AE, Hamilton A, Wang Y, Mach H, Lacroix N, Davis DR, et al. Activation of GATA4 gene expression at the early stage of cardiac specification. Front Chem. 2014;2(MAR):1–8.

102. Bandookwala M, Sengupta P. 3-Nitrotyrosine: a versatile oxidative stress biomarker for major neurodegenerative diseases. Int J Neurosci [Internet]. 2020;130(10):1047–62. Available from: http://dx.doi.org/10.1080/00207454.2020.1713776

103. Ransy C, Vaz C, Lombès A, Bouillaud F. Use of H2O2 to cause oxidative stress, the catalase issue. Int J Mol Sci. 2020;21(23):1–14.

104. Cao G, Fan J, Yu H, Chen Z. Resveratrol attenuates high glucose-induced cardiomyocytes injury via interfering ROS-MAPK-NF-κB signaling pathway. Int J Clin Exp Pathol [Internet]. 2018;11(1):48–57. Available from: http://www.ncbi.nlm.nih.gov/pubmed/31938086%0Ahttp://www.pubmedcentral.nih.gov/articlerender.fcgi?artid=PMC6957970

105. Wu N, Shen H, Liu H, Wang Y, Bai Y, Han P. Acute blood glucose fluctuation enhances rat aorta endothelial cell apoptosis, oxidative stress and pro-inflammatory cytokine expression in vivo. Cardiovasc Diabetol. 2016;15(1):1–13.

106. Wind S, Beuerlein K, Eucker T, Müller H, Scheurer P, Armitage ME, et al. Comparative pharmacology of chemically distinct NADPH oxidase inhibitors. Br J Pharmacol. 2010;161(4):885–98.

107. Li Y, Trush MA. Diphenyleneiodonium an NAD(P)H Oxidase Inhibitor. Biochem Biophys Res Commun. 1998;299:295–9.

108. Riganti C, Gazzano E, Polimeni M, Costamagna C, Bosia A, Ghigo D. Diphenyleneiodonium Inhibits the Cell Redox Metabolism and Induces Oxidative Stress*. J Biol Chem [Internet]. 2004;279(46):47726–31. Available from: https://www.sciencedirect.com/science/article/pii/S0021925820679066

109. Weir EK, Wyatt CN, Reeve HL, Huang J, Archer SL, Peers C. Diphenyleneiodonium inhibits both potassium and calcium currents in isolated pulmonary artery smooth muscle cells. J Appl Physiol. 1994 Jun;76(6):2611–5.

110. Kučera J, Binó L, Štefková K, Jaroš J, Vašíček O, Večeřa J, et al. Apocynin and diphenyleneiodonium induce oxidative stress and modulate PI3K/Akt and MAPK/Erk activity in mouse embryonic stem cells. Oxid Med Cell Longev. 2016;2016.

111. Lang F, Shumilina E, Ritter M, Gulbins E, Vereninov A, Huber SM. Ion channels and cell volume in regulation of cell proliferation and apoptotic cell death. Contrib Nephrol. 2006;152:142–60.

112. Zhang YY, Li G, Che H, Sun HY, Xiao GS, Wang Y, et al. Effects of BKCa and Kir2.1 channels on cell cycling progression and migration in human cardiac c-kit+ progenitor cells. PLoS One [Internet]. 2015;10(9). Available from: http://dx.doi.org/10.1371/journal.pone.0138581

113. Wang L-P, Wang Y, Zhao L-M, Li G-R, Deng X-L. Angiotensin II upregulates K(Ca)3.1 channels and stimulates cell proliferation in rat cardiac fibroblasts. Biochem Pharmacol. 2013 May;85(10):1486–94.

114. Engel FB, Schebesta M, Duong MT, Lu G, Ren S, Madwed JB, et al. p38 MAP kinase inhibition enables proliferation of adult mammalian cardiomyocytes. Genes Dev. 2005;19(10):1175–87.

115. Deschesnes RG, Huot J, Valerie K, Landry J. Involvement of p38 in apoptosis-associated membrane blebbing and nuclear condensation. Mol Biol Cell. 2001;12(6):1569–82.

116. Ma XL, Kumar S, Gao F, Louden CS, Lopez BL, Christopher TA, et al. Inhibition of p38 mitogen-activated protein kinase decreases cardiomyocyte apoptosis and improves cardiac function after myocardial ischemia and reperfusion. Circulation. 1999;99(13):1685–91.

117. Kim D, Sesaki H, Roy S. Reduced levels of drp1 protect against development of retinal vascular lesions in diabetic retinopathy. Cells. 2021;10(6).

118. Ko SH, Choi GE, Oh JY, Lee HJ, Kim JS, Chae CW, et al. Succinate promotes stem cell migration through the GPR91-dependent regulation of DRP1-mediated mitochondrial fission. Sci Rep [Internet]. 2017;7(1):1–14. Available from: http://dx.doi.org/10.1038/s41598-017-12692-x

119. Kishi H, Nakagawa K, Matsumoto M, Suga M, Ando M, Taya Y, et al. Osmotic shock induces G1 arrest through p53 phosphorylation at Ser33 by activated p38MAPK without phosphorylation at Ser15 and Ser20. J Biol Chem. 2001 Oct;276(42):39115–22.

120. Yu-Lee L-Y, Yu G, Lee Y-C, Lin S-C, Pan J, Pan T, et al. Osteoblast-Secreted Factors Mediate Dormancy of Metastatic Prostate Cancer in the Bone via Activation of the TGFβRIII-p38MAPK-pS249/T252RB Pathway. Cancer Res. 2018 Jun;78(11):2911–24.

121. Lafarga V, Cuadrado A, Lopez de Silanes I, Bengoechea R, Fernandez-Capetillo O, Nebreda AR. p38 Mitogen-activated protein kinase- and HuR-dependent stabilization of p21(Cip1) mRNA mediates the G(1)/S checkpoint. Mol Cell Biol. 2009 Aug;29(16):4341–51.

8. Appendix

Appendix A: Methods

A1) Inactivated Mouse Embryonic stem cells (IMEFs) growth curve

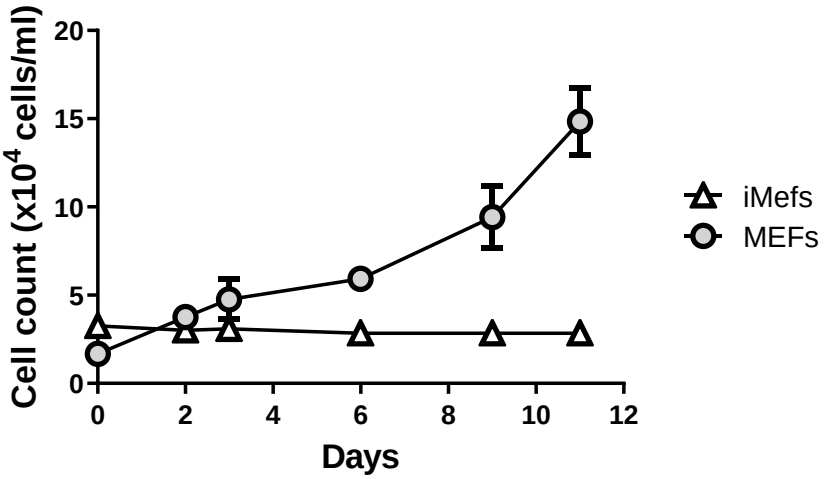

Figure A1: Growth curve of mouse embryonic stem cells (MEFs) versus Inactivated mouse embryonic fibroblasts (iMEFs) (n=3 independent experiments).

A2) Mycoplasma infection test

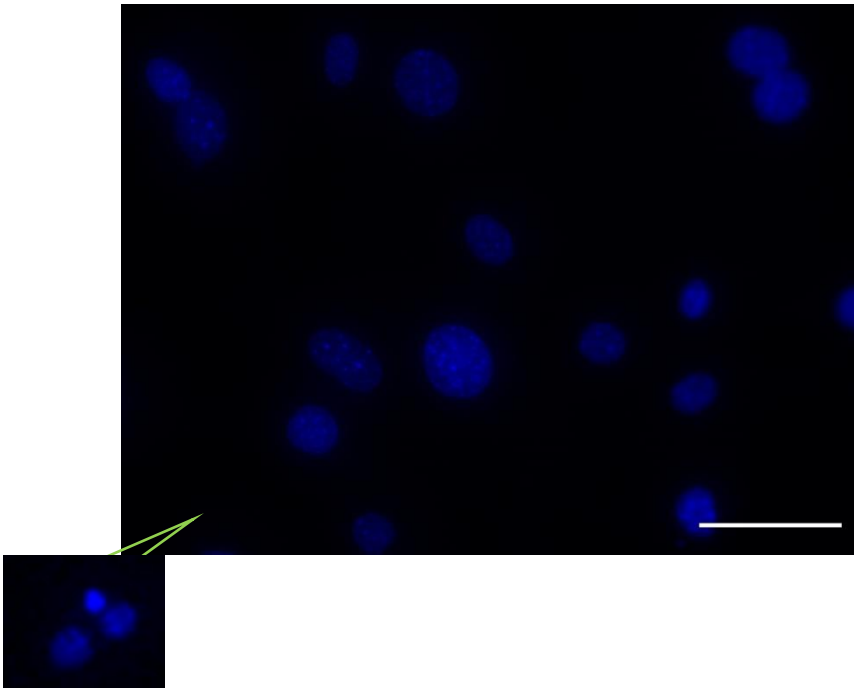

Figure A2: *Representative fluorescence microscopy image of 129 OLA mESCs that have differentiated into cardiac-like cells. The cells were cultured in 25mM media, in the absence of penicillin/streptomycin for 5 days and fixed and stained with Hoechst. Inset, pyknotic nuclei. Imaged at 40x magnification. Cells exhibited no signs of mycoplasma infection. Scale= 50µm.*

A3) Medium supplemented with LIF promote mESC pluripotency

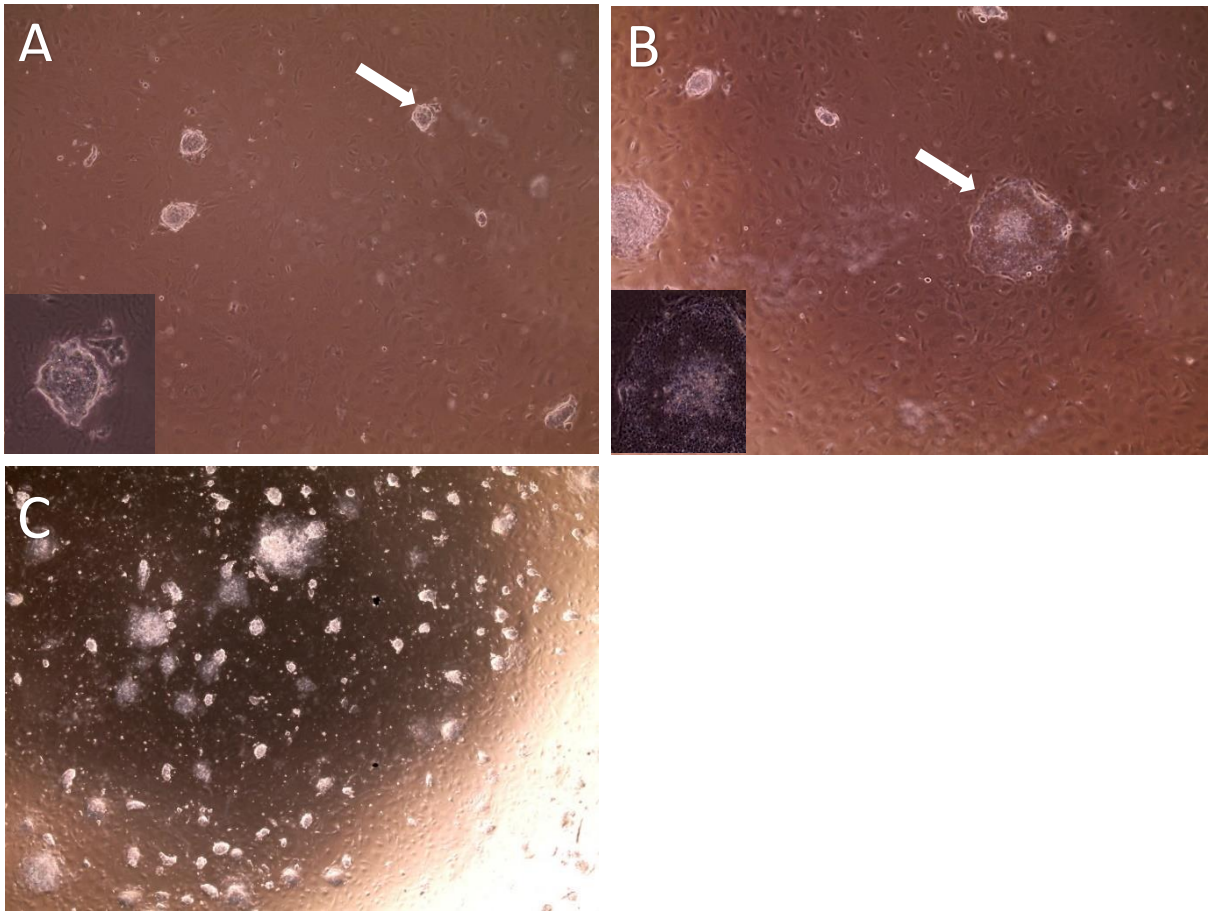

Figure A3: Transmitted light microscopy image of mESCs grown on iMEF feeder layers ***A)*** *Cells retaining pluripotency, forming individual, undifferentiated colonies (4x magnification. Inset at 10x.* ***B)*** *Colonies lost ESC-like morphology, due to overgrowth and self-differentiation (inset 10x magnification), resulted in an amorphous structure being formed.* ***C)*** *Pluripotent mESC (2x magnification) cultured in growth media for 12-16 hours without LIF, arrow (black), mESC colonies loss of defined structure, showing signs of self-differentiation.*

A4) mESC-derived cardiac like generation

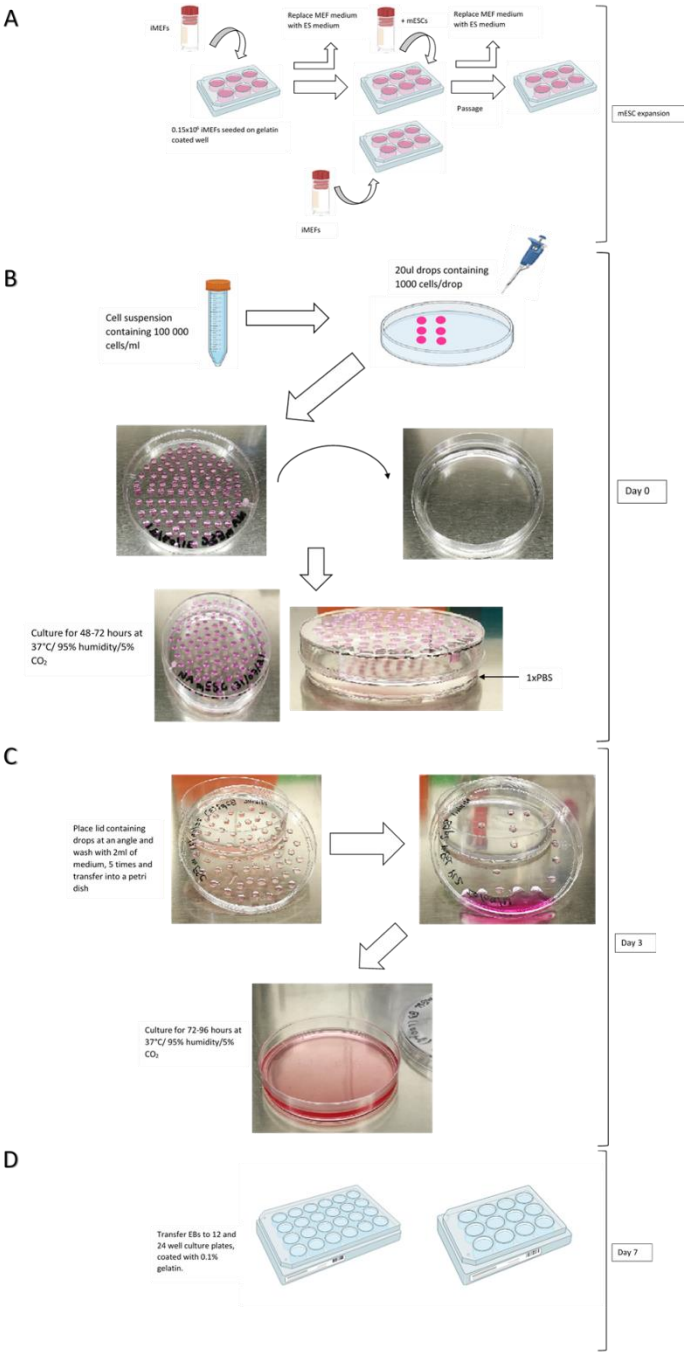

Figure A4: Schematic illustration of the hanging drop protocol for the formation of cardiomyocytes from mESCs. ***A)*** *129 OLA mouse embryonic stem cells (mESCs) are seeded and grown on a feeder of inactivated mouse embryonic fibroblasts (iMEFs) in mESC medium until a 70% cell confluency.* ***B)*** *Expanded mESC cell colonies undergo differentiation using the hanging drop method in 25mM medium for 48-72 hours.* ***C)*** *Drops are flushed by washing with 25mM medium and transferred to a petri dish and incubated for 72-96 hours under standard culture conditions.* ***D)*** *Embryoid bodies are transferred on day 7 of the differentiation protocol to 0.1% gelatin-coated wells. The figure was created using Biorender (https://biorender.com/).*

A5) EB differentiation optimisation

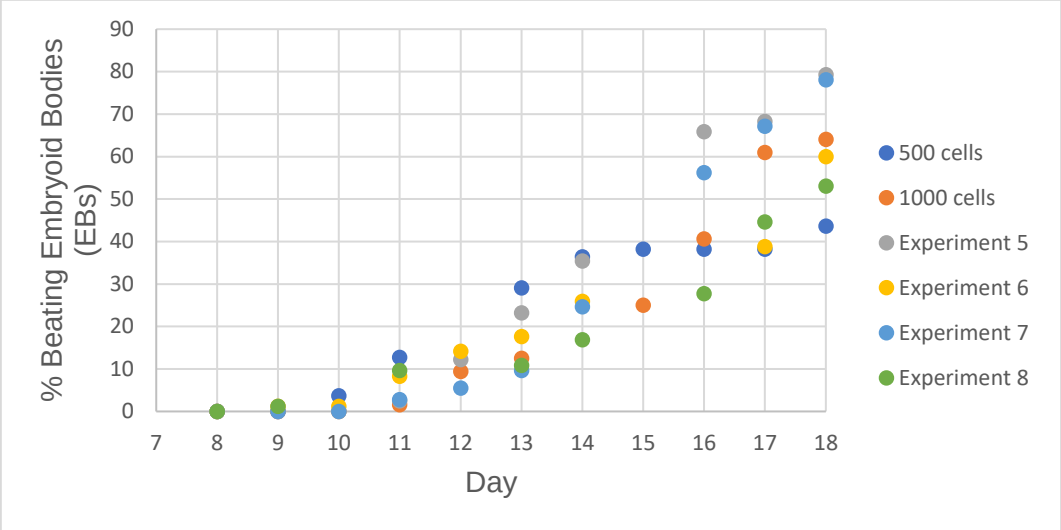

Figure A5: Quantitative analysis expressing the number of beatings EBs relative to the total number of EBs, cultured in 25mM glucose. *Different numbers of cells were seeded in hanging drop formation. At both 500 and 1000 cells/drop. All cells continued to grow and formed spontaneously beating cardiac-like cells, with the onset of beating occurring around the same time. The growth pattern remained consistent, starting with a lag phase between days 8-11where EBs develop outgrowths allowing for adherence to the culture dish, with few EBs exhibiting beating foci. This is followed by an exponential phase between days 12-18 until a plateau, where adherent cells further differentiate and most exhibit spontaneously beating foci. A death phase typically occurred around days 25-27, where differentiated EBs began losing adherence and breaking apart, accompanied by loss of beating activity – this, however, could be due to a lack of nutrients and overgrowth.*

Table 2. Preparation of protein standards for standard curve

Concentration	Diluent (RIPA) (µl)	Source of BSA (µl)
2000	0	300 of 2000µg stock
1000	325	325 of 2000µg stock
500	325	325 of 1000µg
125	325	325 of 250µg
0 (Blank)	400	0

Table 3: Western Blot reagents

Reagent	Constituents
4x Transfer Buffer	43g Tris Buffer 109.45g Glycine Make to 2L dH2O
1x Transfer Buffer	250ml 4xTransfer Buffer 200ml Isopropanol Make up to 1L dH2O
Dithiothreitol (DTT)	1M solution prepared: 1.55g DTT powder 10ml deionized H2O Filter to sterilize
10 x PBS	80g NaCl (1.37M) 2g KCl (27mM) 17.8g Na2HPO4.dH2O (100mM) 2.4g KH2PO4 (18mM)
Ponceau S. Stain	1g Ponceau S. 50ml acetic acid Make to 1L ddH2O

Table 4. Resolving gel and stacking gel constituents used in SDS page for protein separation.

Resolving Gel (10%)		Stacking Gel (5%)	
Constituent	Final concentration	Constituent	Final concentration
H2O	-	H2O	-
40% acrylamide	10%	40% acrylamide	10%
1.5M Tris pH 8.8	0.375M	1.5M Tris pH 6.8	0.1875M
10% SDS (Sodium dodecyl-sulfate)	0.1%	10% SDS (Sodium dodecyl-sulfate)	0.1%
10% APS (ammonium persulfate)	0.1%	10% APS (ammonium persulfate)	0.1%
VORTEX			
TEMED (Tetramethylethylenediamine)	0.1%	TEMED (Tetramethylethylenediamine)	0.1%
VORTEX			

A6) Ponceau S. Stain

Figure A6: Representative PVDF membrane while destaining Ponceau S stain. The e*fficacy of protein transfer was tested by incubating the membrane with Ponceau S stain in the dark for 5 min at room temperature. Following rapid washing with H_2O, faint bands started to appear. 10µg protein sample loaded wells 2 and 3.*

Appendix B: Results

B1) Typical developmental pattern of EB

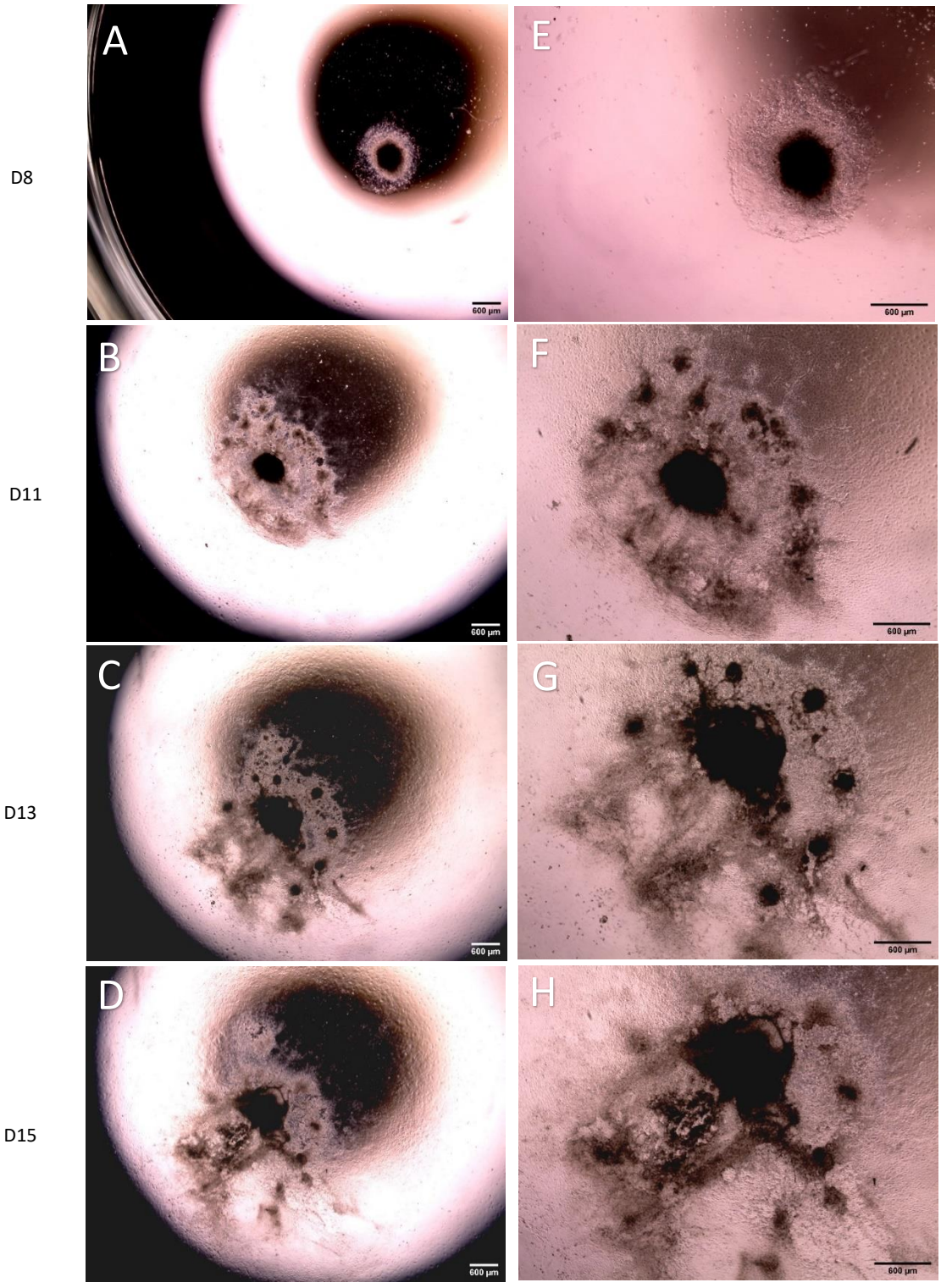

Figure B1: Transmitted light microscopy images showing the typical developmental pattern of an embryoid body (EB) cultured in baseline glucose (25mM) conditions at different time points. EB differentiated and exhibited spontaneously beating foci from day 11. 2x objective (A-D) and 4x objective (E-H). Scale=600µm. Images generated using EVOS XL Core.

B2) Effect of oxidative stress on beating activity

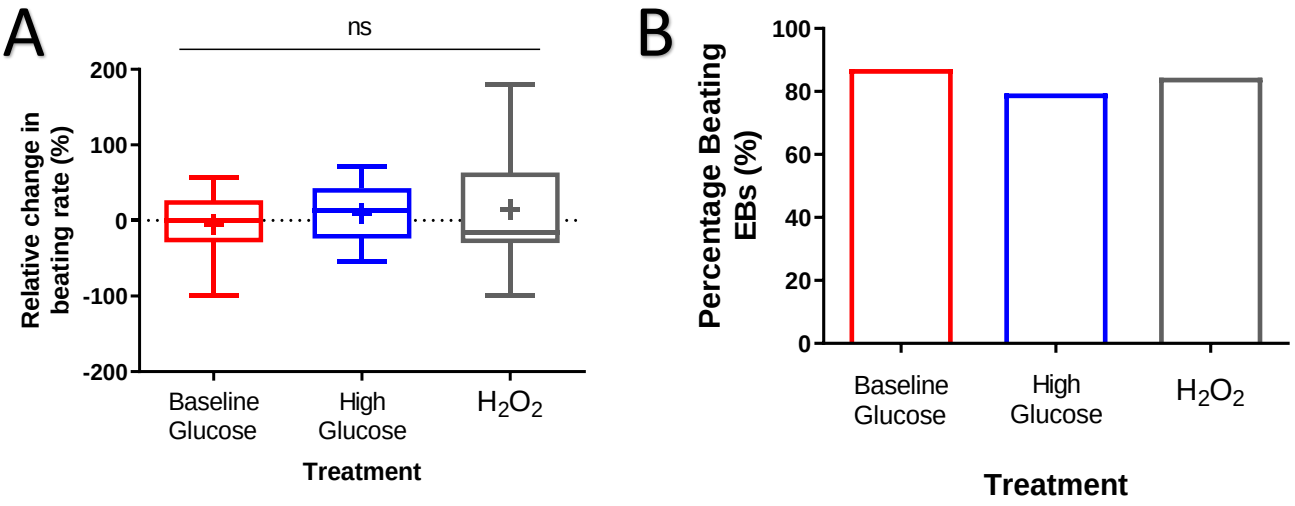

Figure B2: Functional effects of hyperglycaemic-induced oxidative stress on stem cell-derived cardiac-like cells. ***A)*** *Quantitative analysis of relative change in EB diameter (n=3 independent cell culture batches, n≥10 EBs per group). Data is represented as a box-and-whisker plot, with the mean depicted as "+"* ***B)*** *Quantitative analysis of percentage beating EBs, (expressed relative to total) post-treatment (n=3 independent cell culture batches for each treatment and ≥31 EBs per group).*

B3) Effect of NOX inhibition on cell proliferation and functional activity

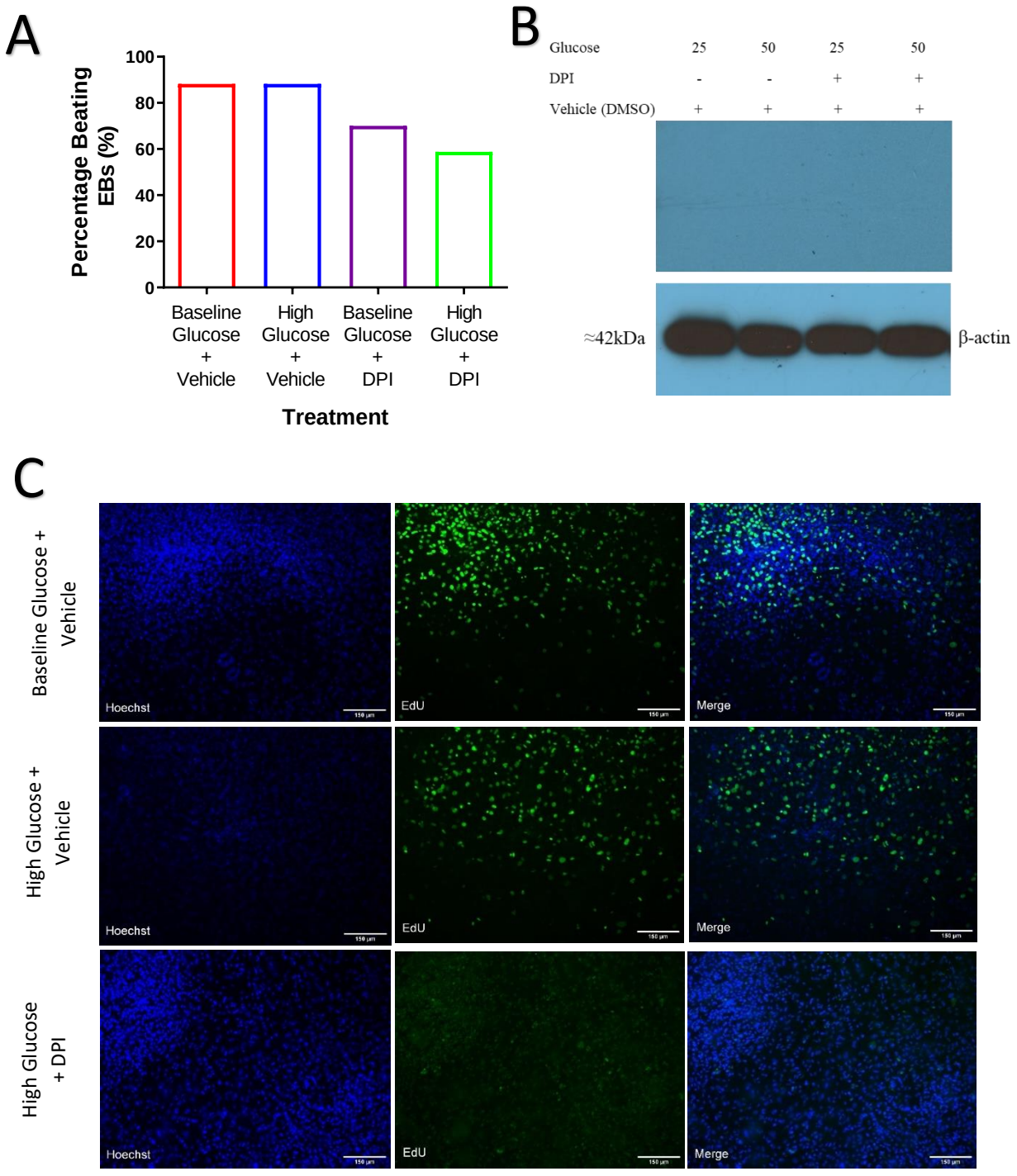

Figure B3: **Effect of the pharmacological inhibition of NOX on cell proliferation and beating activity.** ***A)*** *Quantitative analysis of percentage beating EBs relative to (n=2 independent cell culture batches for each treatment and ≥9 EBs per group).*
B) *Representative western blot of nitrotyrosine (protein damage marker), and β-actin, set as control (n=2).* ***C)*** *Representative fluorescence microscopy images of Hoechst (Blue), EdU*

(green), and merged images (10x magnification). Scale bar = 150μM. (n=2 independent cell culture batches, with n=2-3 EBs per group).

B4) Effect of p38 MAPK inhibition on beating activity

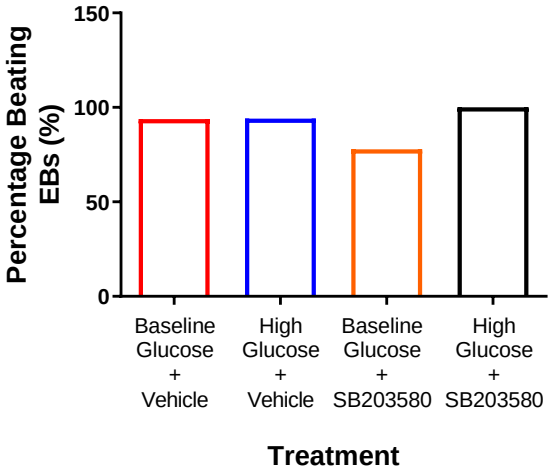

Figure B4: Effect of the pharmacological inhibition of p38 MAPK on beating activity. *Quantitative analysis of percentage beating EBs relative to (n=3 independent cell culture batches for each treatment and ≥9 EBs per group).*

B5) Cell viability

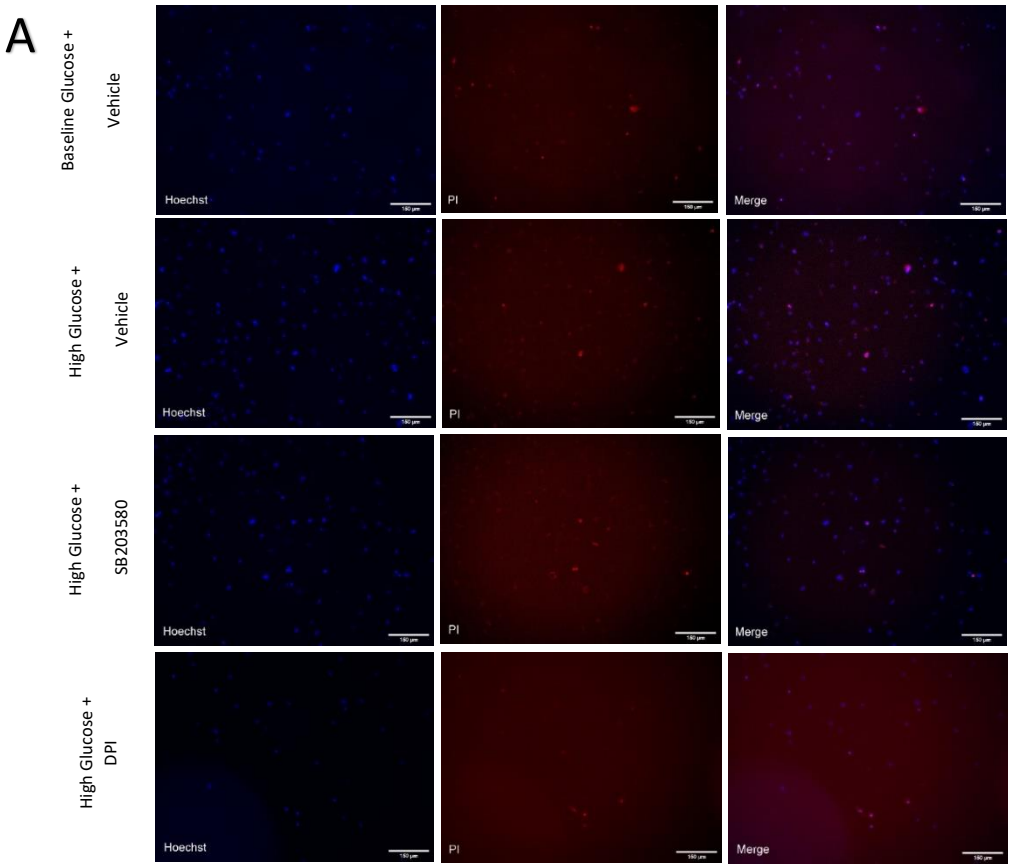

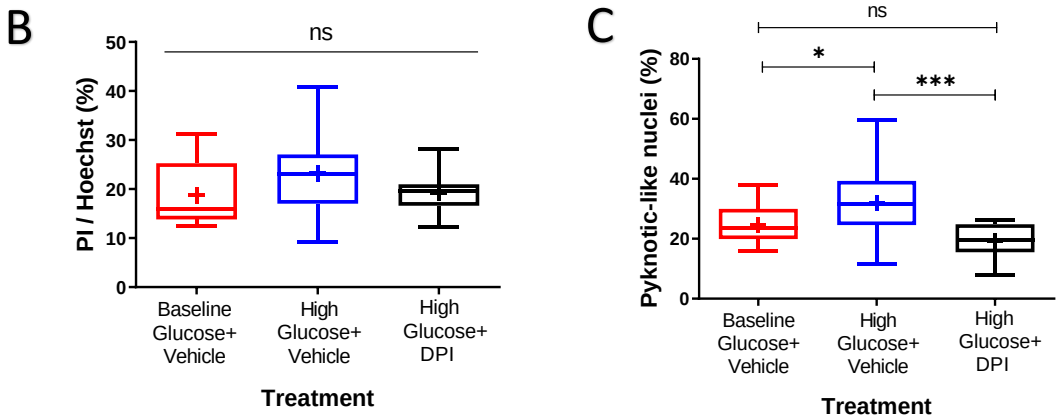

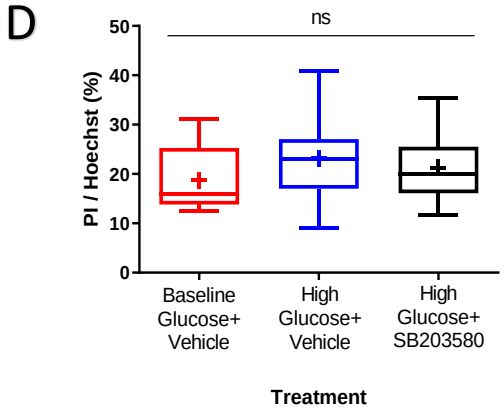

Figure B5: Effect of pharmacological inhibition of NOX and p38 MAPK on cell survival. ***A)*** *Representative immunofluorescence images of Hoechst (Blue), Propidium iodide (Red), and merged images (10x). Scale bar = 150µm.* ***B-C)*** *Quantitative analysis of the %PI positive cells or %Pyknotic-like nuclei relative to total (n=2 independent cell culture batches, n=3-8 EBs per group)* ***D)*** *Quantitative analysis of the %PI positive cells relative to total (n=3 independent cell culture batches, with n=4-8 EBs per group).* ***B-D)*** *Data represented as a box and whisker plot, with the mean shown as "+" with significant (*P≤0.05, **P≤0.01, ***P≤0.001) compared to baseline glucose.*

B6) Effects p38 MAPK inhibition on GATA4 expression

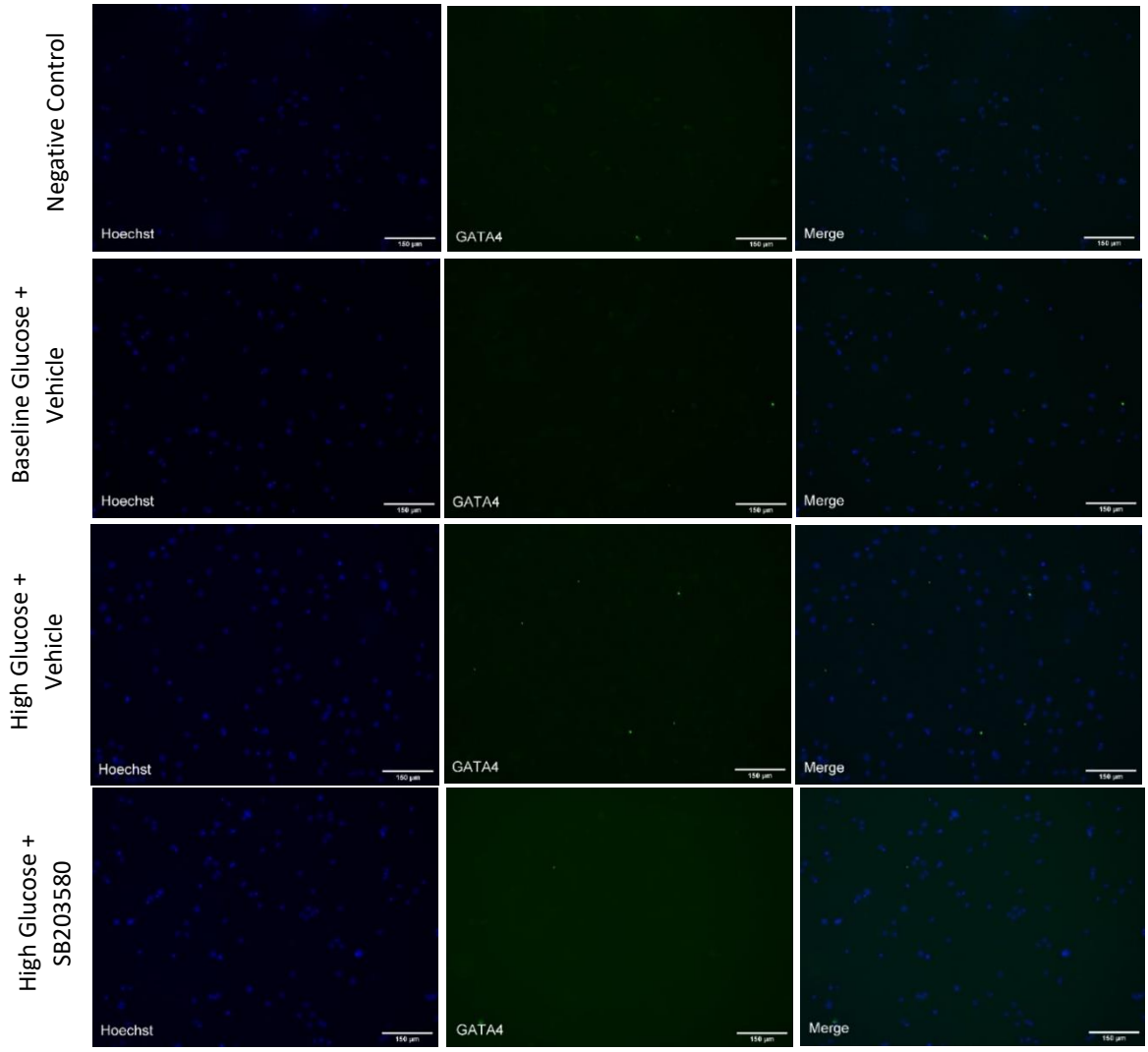

Figure B6: Effect of the pharmacological inhibition of p38 MAPK on cardiac maturation. *Representative fluorescence microscopy images of Hoechst (Blue), GATA4 (green), and merged images (10x magnification). Scale=150µm. (n=2 independent culture batches, with n=2-3 EBs per group).*